

170355

ALL OPTICAL SWITCHING VIA  
DIFFRACTION GRATING FORMED BY  
INTERFERENCE OF GAUSSIAN BEAMS

A Thesis Submitted to  
The Graduate School of Engineering and Sciences of  
İzmir Institute of Technology  
in Partial Fulfillment of the Requirements for the Degree of

MASTER OF SCIENCE

in Electrical & Electronics Engineering

by  
Osman AKIN

January 2005  
İZMİR

- Luo, H.J., Zory, P.S., 1990. "Distributed Feedback Coupling Coefficient in Diode Lasers with Metallized Gratings", IEEE Photonics Technology Letters, Vol.2, No:9
- Masanovic, G.Z., Passaro, V.M.N., Reed, G.T, 2003. "Dual Grating Assisted Directional Coupling Between Fibers and Thin Semiconductor Waveguides", IEEE Photonics Technology Letters, Vol.15, No:10
- Park, S., Song, H.H., Oh, C.H., Kim, P.S., 2001. "Ray Optical Determination of The Coupling Coefficients of Grating Waveguide by Use of the Rigorous Coupled Wave Theory", Journal of Lightwave Technology, Vol.19, No:1
- Ranka, J. K., Gaeta, A.L., Baltuska, A., Pshenichnikov, M.S, Wiersma, D.A., 1997. "Autocorrelation Measurement of 6 fs Pulses Based on the Two Photon Induced Photocurrent in a GaAsP Photodiode", Optics Letter, Vol. 22, No:17.
- Reid, D.T., Padgett, M., McCowan, C., Sleat, W., Sibbet, W., 1997. "Light Emitting Diodes as Measurement Devices for Femtosecond Laser Pulses", Opt. Lett., Vol.22, p.233.
- Schneider, T., Wolframm, D., Mitzner, R., Reif, J. 1999. "Ultrafast optical switching by instantaneous Laser Induced Grating Formation and Self Diffraction in Barium Fluoride", Appl. Phys. B 68,749-751.
- Schneider, T., Schmid, R.P, Reif, J. 2001. "Efficient Self Phase Matched Third Harmonic Generation of Ultrashort Pulses in a Material with Positive Dispersion", Appl. Phys. B
- Schneider, T., Wolframm, D., Reif, J. 2000. "Ultrafast Laser Induced Index Grating in Transparent Insulators", Nuclear Instruments and Methods in Physics Research B, Vol. 166-167, 808-814
- Schneider, T., Schmid, R.P, Reif, J. 2002 "Femtosecond Third Harmonic Generation:

We approve the thesis of **Osman AKIN**

**Date of Signature**



**Assist. Prof. Dr. M.Salih DİNLEYİCİ**  
Supervisor  
Department of Electrical and Electronics Engineering  
İzmir Institute of Technology

**17 January 2005**



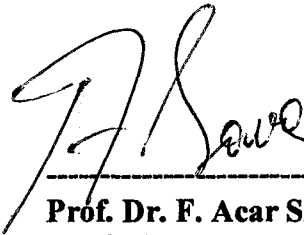
**Assist. Prof. Dr. Alp KUŞTEPELİ**  
Department of Electrical and Electronics Engineering  
İzmir Institute of Technology

**17 January 2005**



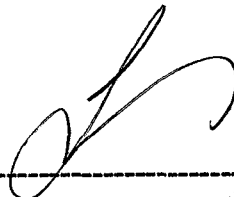
**Assist. Prof. Dr. Sami SÖZÜER**  
Department of Physics  
İzmir Institute of Technology

**17 January 2005**



**Prof. Dr. F. Acar SAVACI**  
Head of Department  
İzmir Institute of Technology

**17 January 2005**



**Prof. Dr. Semra ÜLKÜ**  
Head of Graduate School

## ACKNOWLEDGMENT

I would like to thank my supervisor Asst. Prof. Dr. M. Salih Dinleyici for his guidance, support and encouragement throughout my research. He spent a significant amount of time supervising this work and always had time for my questions.

I am grateful to Asst. Prof. Dr. Alp Kuştepe and Asst. Prof. Dr. Sami Sözüer for serving on my thesis committee.

I am deeply indebted to Fulya Karagöz for her love and emotional support. I would like to thank my parents and my sisters for their invaluable support throughout my life.



## ABSTRACT

In this study we investigate an all-optical switching node which can be controlled via transient grating formed by interference of two Gaussian beams. This design considers 3-D architecture of switching fabrics, real profile of Gaussian beams and nonlinearity for fast switching time requirements. Four Wave Mixing (FWM) is applied in the evanescent field region of waveguide to estimate the reflection angle and the efficiency of switching node. The effect of the formed grating on the propagation of mode is analysed by coupled mode theory and co-directional mode coupling coefficient is found by using Distributed Feedback Laser approach. A method for overall diffraction efficiency is proposed and optimization parameters for better efficiency are described.



## ÖZET

Bu çalışmada iki Gauss hüzmesinin girişimi ile oluşturulan, geçici kırınım ızgarasıyla kontrol edilen tamamen optik anahtarlama düğümü incelenmiştir. Bu tasarımda 3 boyutlu anahtarlama örgüsü, Gauss hüzmelerinin gerçek profili ve hızlı anahtarlama süreleri için malzemelerin doğrusal olmayan tepkileri düşünülmüştür. Yansıma katsayısını ve anahtarlama düğümünün verimini bulabilmek için dalga kılavuzun sönümlü bölgesine dört dalga karışımı metodu uygulanmıştır. Oluşturulan ızgaranın yayılma kipi üzerindeki etkisi kuple dalga denklemleri ile incelenmiş ve kuple katsayısı Dağıtık Geri Beslemeli Lazer yaklaşımıyla hesaplanmıştır. Toplam kırınım verimliliği için bir yöntem önerilmiş ve daha yüksek verimlilik için optimizasyon parametreleri açıklanmıştır.



# TABLE OF CONTENTS

LIST OF FIGURES.....	vii
LIST OF TABLES.....	ix
CHAPTER 1. INTRODUCTION.....	1
CHAPTER 2. OPTICAL MATERIALS FOR PHOTONIC SWITCHING AND THIRD ORDER NONLINEARITIES.....	4
2.1 Third Harmonic Generation.....	5
2.2 Optical Kerr Effect.....	6
2.3 Two Photon Absorption .....	8
2.4 Four Wave Mixing.....	11
CHAPTER 3. OPTICAL WAVEGUIDES AND ANALYSING TECHNIQUES FOR GRATING ASSISTED COUPLERS.....	13
3.1 Propagation of Light in Waveguides.....	13
3.1.1 Ray Approach: Total Internal Reflection and Frustrated Internal Reflection.....	13
3.1.2 Wave Approach : Waveguide Modes in a Slab Waveguide.....	14
3.2 Perturbation Analysis of Corrugated Periodic Waveguide.....	16
3.3 Distributed Feedback Laser Approach .....	23
3.4 Photonic Crystals.....	25
CHAPTER 4 ALL OPTICAL SWITCHING NODE.....	29
4.1 Introduction.....	29
4.2 The Switching Node Model.....	30
4.3 Deflection Angle Calculation.....	31
4.4 Three Dimensional GratingFormation.....	35
4.4.1 General Expression For a Gaussian Beam.....	35
4.4.2 Grating Formation By Interference of Two Gaussian Beams Traveling in Arbitrary Directions.....	36
4.4.3 First Order Approximation.....	42

4.5 Coupled Wave Equations.....	46
4.6 Overall Efficiency Using DFB Approach.....	48
CHAPTER 5. MEASUREMENTS AND EXPERIMENTAL STUDIES.....	52
5.1 Autocorrelation Principles.....	52
5.2 Two Photon Absorption in Semiconductor Photodiodes.....	54
CHAPTER 6. CONCLUSION.....	57
REFERENCES.....	59





# LIST OF FIGURES

<u>Figure</u>		<u>page</u>
Figure 1.1	General Switching Node.....	2
Figure 2.1	Third Harmonic Generation.....	6
Figure 2.2	Four Wave Mixing Process.....	12
Figure 3.1	Total and Frustrated Internal Reflection.....	13
Figure 3.2	The Field Distributions Corresponding To The Different Value Of $\beta$ ....	15
Figure 3.3	A Corrugated Periodic Waveguide.....	19
Figure 3.4	The Incident and Reflected Intensities in the Corrugated Section.....	22
Figure 3.5	Typical Grating Waveguide Device.....	24
Figure 3.6	One Dimensional Photonic Crystal.....	25
Figure 3.7	Dispersion Relation For a 1D Photonic Crystal.....	28
Figure 4.1	Nodes in Single Line All Optical Switch Fabric.....	29
Figure 4.2	The Transient Grating Formation On the Side of a Waveguide and Grating Assisted Directional Coupler.....	31
Figure 4.3	FWM at The Core – Cladding Boundary.....	32
Figure 4.4	Interference Geometry Of Gaussian Beams.....	37
Figure 4.5	Interference Pattern Formation and Comparison of Gratings For Different Gaussian Beam Parameters.....	42
Figure 4.6	Grating Fronts.....	46
Figure 4.7	Gaussian Grating Structure.....	49
Figure 4.8	Dependence Of Diffraction Efficiency On The Incidence Angle $\phi$ .....	51
Figure 5.1	Basic Michelson Interferometer.....	52
Figure 5.2	Two Photon Absorption Experiment Setup.....	54
Figure 5.3	Autocorrelator Experiment Setup.....	55

# LIST OF TABLES

<u>Table</u>		<u>page</u>
<b>Table 2.1</b>	Third Order Nonlinear Susceptibilities.....	<b>8</b>
<b>Table 2.2</b>	Two Photon Absorption Coefficients.....	<b>10</b>



# CHAPTER 1

## INTRODUCTION

The needs for processing data in higher rates encourage researchers to investigate more enhanced information processing devices and systems. Recent electronic devices have reached their limits and they are being replaced by equivalent optical components to satisfy the demand for higher speed operations. At present, signal processing operations like switching and routing are carried out electronically. Traditional optical fiber network architecture requires optical – electronic – optical conversion at each node that reduces data processing rates and increases operational cost. Alternatively, an all optical switches and routers can be designed and implemented to eliminate that drawbacks of current communication systems. The optical switches can be used in a wide range of applications for optical circuit or packet switching. Wavelength selective switches can be used to add and drop specific wavelength from multi-wavelength signals (add-drop multiplexing) and to monitor the specific signal in defined wavelength in order to manage the network.

To be useful for all optical switching, materials should have a large nonlinear refractive index, ultrafast responses to an applied optical field and minimum absorption loss. Optical Kerr effect in optical materials is one of the fastest phenomenon that can be exploited in designing an ultrafast all optical switch. Some symmetric and nonsymmetric Kerr type materials exhibit almost instantaneous response time of  $10^{-15}$  that makes them very suitable for ultrafast optical switching. Photorefractive effect is the another phenomenon that has been utilized in all optical signal applications for a long time. When photorefractive material is illuminated with optical field, an electric charge is produced and carriers migrate due to drift and diffusion. This mobility causes a strong space - charge field that induces a refractive index change by the Pockels effect. Because of the charge migration, photorefractivity is rather slow process in the order of  $10^{-8}$  s, which is not good for today's all optical switching requirements of about 100 Gbits/s. Nevertheless, photorefractive materials have large optical nonlinearity and can hold the information for a long time that is more convenient for volume holography or neural network applications rather than switching applications.

In this thesis we propose and analyse the design of an all optical switching node

based on the transient grating, which is formed by interference of two Gaussian beams. For this purpose we utilize third optical nonlinearity [ $\chi^{(3)}$ ] phenomenon exhibited in nonlinear optical materials. The proposed design aims to extract propagating light from a waveguide and transfer it into another as fast as possible. In order to achieve that goal, a transient grating is produced in cladding region of the waveguide, as shown in figure 1.1.

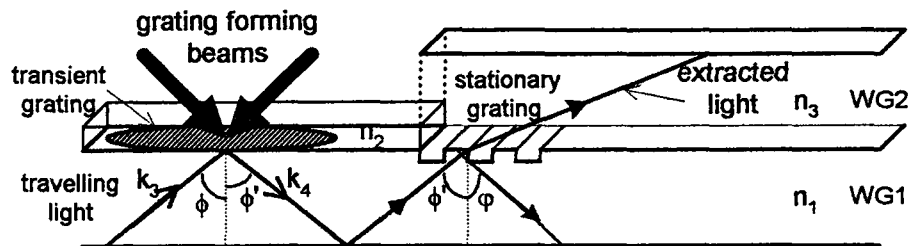


Figure 1.1 General Switching Node

This grating changes the propagating properties of waveguides by destroying the requirements of the total internal reflection of the mode. The evanescent field in the cladding side of the waveguide and the grating forming beams interacts in the grating region and this event can be mathematically analyzed via Four Wave Mixing. Combination of Four Wave Mixing process with ray optics method gives us opportunity to find some parameters of the reflected mode, such as the new propagation angle and mode coupling coefficient. Finally, by using second stationary grating, it is possible to extract the destroyed mode into the second waveguide with a high efficiency.

In this design, the diffraction efficiency of the general purpose switching node strongly depends on the parameters of transient grating. The structure of the grating is defined by the interference pattern of two non-collinear waves and this structure can be easily changed by modifying the Gaussian beam parameters. Nevertheless, the intensities of grating generating beams must be above of some threshold value. Otherwise, the interference pattern does not produce any transient grating and the Four Wave Mixing process reduces to an energy coupling mechanism from the stronger beam to the weaker one.

This thesis is separated into four principal chapters describing respectively the third order optical nonlinearity, optical waveguides, ultrashort pulse width measurement and all optical switching node.

In chapter 2, we establish a background for materials and phenomena that may be employed in designing an ultrafast all optical switch. In this section we introduce third order optical nonlinearity and illustrates how nonlinear media response to an applied strong optical field. Our aim is to give a comprehensive knowledge about methods for modulating the refractive index of the medium and interaction of three waves inside a nonlinear material.

In Chapter 3, we describe the propagation of light in waveguides and analyse it by using ray and wave optics approach. Also, we explain the standard methods for studying corrugated waveguides and give a general solution to coupling of forward modes to backward. We define the coupling coefficient by using Distributed Feedback Laser model.

In Chapter 4, we show how Two Photon Absorption can be used to measure the pulsewidth of an ultrashort pulse. In this section we derive a mathematical expression for the photocurrent resulted from TPA process in photodiode that is illuminated by pulse signal.

Finally, in Chapter 5, we describe a switching node, that is based on transient grating formed by interference of two Gaussian beams. The contribution of this thesis will be to develop a ray optics formalism to estimate the reflection angle, and wave optics approach to find the overall efficiency of the system by considering the Four Wave Mixing process during the interaction of grating waves with evanescent waves in the core-cladding boundary of the waveguide.

## CHAPTER 2

### OPTICAL MATERIALS FOR PHOTONIC SWITCHING AND THIRD ORDER NONLINEARITIES

The origin of the optical nonlinearity lies in the nonlinear response of an optical material to an applied strong optical field ( laser beam ). The properties of a dielectric medium through which an optical wave propagates can be described by the relation between the polarization density vector  $P(r,t)$  and the electric field vector  $E(r,t)$ . In isotropic, homogeneous and dispersionless medium, the relation between  $P(r,t)$  and  $E(r,t)$  can be written in the form(Saleh 1991)

$$P = \epsilon_0 \chi E + 2dE^2 + 4\chi^{(3)}E^3 + \dots \quad (2.1)$$

where  $\chi$  is the linear susceptibility,  $d$  and  $\chi^{(3)}$  are known as the second order and third order nonlinear optical coefficient, respectively.

The polarization density  $P$  can be written as a sum of linear and nonlinear parts

$$P = \epsilon_0 \chi E + P_{NL}$$

where

$$P_{NL} = 2dE^2 + 4\chi^{(3)}E^3 \quad (2.2)$$

Thus, by using Maxwell's equation, one can derive the propagation of light in a nonlinear medium, that may be written in the following form

$$\nabla^2 E(r,t) - \frac{1}{c^2} \frac{\partial^2 E(r,t)}{\partial t^2} = \mu_0 \frac{\partial^2 P_{NL}(r,t)}{\partial t^2} \quad (2.3)$$

Regarding to eq. (2.3), the nonlinear polarization density  $P_{NL}$  can be considered as the source of the nonlinearity in the optical materials.

The first term on the right side of eq.(2.2), that is  $P^{(2)}(t) = 2dE^2$ , stands for the second order optical nonlinearity and phenomena like second harmonic generation, sum and difference frequency mixing, three wave mixing and optical Pockel effect are related with this term. This nonlinearity can be observed only in noncentrosymmetric medium and typical values for the second order nonlinear coefficient lie in the ranges  $10^{-24}$  to  $10^{-21}$  (MKS units, A-s/V<sup>2</sup>) (Saleh 2001). Although second order nonlinear materials have a higher nonlinearity constant than third order materials, they are not very suitable for all optical switching applications. First of all, optical glasses recently used in optical waveguides are centrosymmetric materials and do not possess second order nonlinearity. But recently it was shown that a glass, doped with Germanium and Phosphorus can generate a second harmonic generation (Margulis 1987). On the other hand, response time of the second order nonlinear material is about 1 ps (Nahata 1996), which is slow compared with femtosecond time responses of third order materials (Zhang 2003). Furthermore, refractive index modulation is a key parameter in estimating the diffraction efficiency of the switching node and Aitchison et.al 1997 demonstrated experimentally about 17% modulation of the second order coefficient, while the third order coefficient was changed about 50%. In consequence, second order medium exhibiting efficient switching seems to remain an active area of research.

Third order nonlinear effect is the phenomenon that lies under the all optical switch idea, proposed and analysed in this thesis. Third order nonlinearities lead to intensity dependencies of refractive index or absorption coefficient that offer a chance to control the propagation of light beams by purely optical means. There are several phenomena that are useful to characterize the third order nonlinear processes such as third harmonic generation, optical Kerr effect, four wave mixing and two photon absorption.

## 2.1 Third Harmonic Generation

To understand better third harmonic generation phenomenon, let us consider the second term of nonlinear polarization density  $P$  in eq. (2.2)

$$P^{(3)} = 4\chi^{(3)}E^3(t) \quad (2.4)$$

The electric field can be written as  $E(t) = E(\omega) \cos(\omega t)$ . When we place this definition into eq. (2.4) we obtain

$$P^{(3)}(t) = P(\omega, t) + P(3\omega, t) = 3\chi^{(3)}E^3(\omega) \cos(\omega t) + \chi^{(3)}E^3(\omega) \cos(3\omega t) \quad (2.5)$$

The second term on the right side of the polarization equation indicates the generation of the third harmonic of the input field. This fact is illustrated better in Figure 2.1.

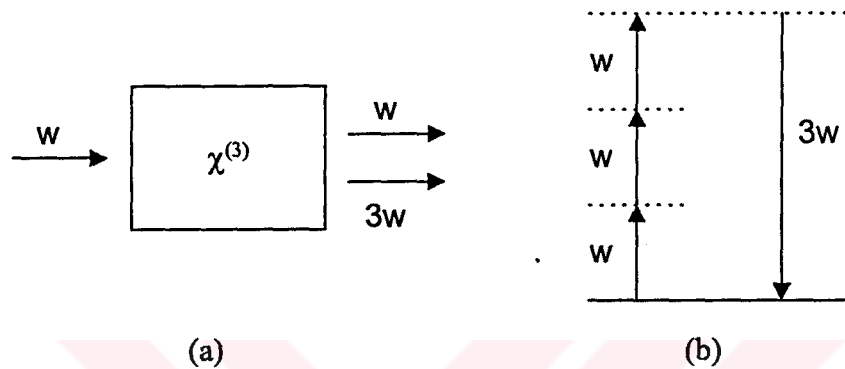


**Figure 2.1** Third harmonic generation

a) Geometry of the interaction b) Energy level description

This process can be described by using quantum optics as three photons of frequency  $\omega$  are absorbed and one photon of frequency  $3\omega$  is created. In fact, it is important to note that the first term of eq.(2.5) is capable of changing the refractive index of the medium, that is the so-called Optical Kerr Effect.

## 2.2 Optical Kerr Effect

The nonlinear polarization density can also be defined as (Saleh 2001)

$$P_{NL}(\omega) = \epsilon \Delta\chi E(\omega) \quad (2.6)$$

Let us assume that third order effect is dominant nonlinearity in the medium and then the polarization component responsible for optical Kerr effect in eq.(2.5) can be rewritten as



$$P_{NL}^{(3)} = 3\chi^{(3)}|E(\omega)|^2 E(\omega) \quad (2.7)$$

From eq. ( 2.6 ) we know that

$$\varepsilon \Delta\chi = \frac{P_{NL}^{(3)}}{E(\omega)} = 3\chi^{(3)}|E(\omega)|^2 \quad (2.8)$$

If we assume that intensity is defined as  $I = \frac{|E(\omega)|^2}{2\eta}$  and plugin into eq. (2.8) , we obtain

$$\Delta\chi = \frac{6\chi^{(3)}\eta}{\varepsilon_0} I \quad (2.9)$$

where  $\eta$  is the impedance of the medium. We know that refractive index of the medium is defined as  $n^2 = 1 + \chi$  and  $\Delta n = \frac{\partial n}{\partial \chi} \Delta\chi$ . By using this definitions we obtain refractive index change as

$$\Delta n = \frac{\Delta\chi}{2n} \quad (2.10)$$

When we replace susceptibility change  $\Delta\chi$  with that obtained in eq. ( 2.9 ) we find that refractive index is modulated by the intensity of the input beam

$$\Delta n = \frac{3\eta\chi^{(3)}}{\varepsilon_0 n} I \quad (2.11)$$

The impedance of the dielectric medium is defined as  $\eta = \sqrt{\frac{\mu}{\varepsilon}} = \sqrt{\frac{\mu_r \mu_0}{\varepsilon_r \varepsilon_0}} = \frac{\sqrt{\mu_0}}{\sqrt{\varepsilon}} = \frac{\eta_0}{n}$

for  $\mu_r=1$ .

Then the refractive index change can be written as

$$\Delta n = \frac{3\eta_0}{n^2 \varepsilon_0} \chi^{(3)} I \quad (2.12)$$

According to this equality, Kerr coefficient is defined as

$$n_2 = \frac{3\eta_0}{n^2 \epsilon_0} \chi^{(3)} \quad (2.13)$$

where  $\chi^{(3)}$  is assumed to be real value.

During the derivation of this coefficient we assume that the medium is nonresonant i.e the energy of photons of applied optical field is much smaller than bandgap. This is non-resonant nonlinearity situation and materials that own this property exhibit a nearly instantaneous response time on the order of femtoseconds. However, the induced nonlinear index changes are often very small. In table 2.1 the experimentally measured values of nonlinear susceptibilities are given(Boyd 1992).

<i>Material</i>	$\chi^{(3)}$	<i>Response Time</i>
Air	$1.2 \times 10^{-17}$	
Carbon Disulfide	$1.9 \times 10^{-12}$	2 ps
GaAs	$6.5 \times 10^{-4}$	20 ns
GaAs / GaAlAs ( MQW )	0.04	20 ns
Indium antimonide	0.3	400 ns
Semiconductor doped glass	$10^{-8}$	30 ps
Optical glasses	$(1-100) \times 10^{-14}$	Very fast
Polydiacetylene	$2.5 \times 10^{-10}$	Very fast

**Table 2.1** Third Order Nonlinear Susceptibilities

### 2.3 Two Photon Absorption ( TPA )

In general third order nonlinear susceptibility ( $\chi^{(3)}$ ) has a real part responsible for the nonlinear refraction and an imaginary part, responsible for the nonlinear absorption [REZA]. In order to find TPA coefficient  $\beta$ , let us write the wave equation in nonlinear medium, i.e eq. (2.3) in frequency domain. It is easy to write

$$\nabla^2 E(r, \omega) + \frac{\omega^2}{c^2} E(r, \omega) = -\mu_0 \omega^2 P_{NL}(r, \omega) \quad (2.14)$$

Let us assume that we have a wave, propagating in z direction and linearly polarized in the x direction. Then, we can write electric field vector as

$$E(\mathbf{r}, \omega) = E(z, \omega) = A(z)e^{-jkz} \quad (2.15)$$

The nonlinear polarization density component responsible for TPA can be written as that in eq. (2.7), where it is

$$P_{NL}^{(3)} = 3\chi^{(3)}|E(z, \omega)|^2 E(z, \omega) \quad (2.16)$$

Substituting eq.(2.15) and eq.(2.16) into eq.(2.14) leads to

$$\frac{\partial^2 E(z, \omega)}{\partial z^2} + \frac{\omega^2}{c^2} E(z, \omega) = -3\mu_0 \omega^2 \chi^{(3)} E(z, \omega) |E(z, \omega)|^2 \quad (2.17)$$

Consider that electric field is plane wave, then we can write

$$E(z, \omega) = A(z)e^{-jkz} \quad (2.18)$$

By combining eq.(2.18) and eq.(2.17), and assume that second order terms are slowly varying, we obtain

$$\frac{dA}{dz} = \frac{3\mu_0 \omega^2 \chi^{(3)}}{2jk} A(z) |A(z)|^2 \quad (2.19)$$

We know that susceptibility consists of real and imaginary parts

$$\chi^{(3)} = \chi_{re}^{(3)} + j\chi_{im}^{(3)} \quad (2.20)$$

and the imaginary term will give the TPA coefficient. Thus, we are interested only with imaginary term. Therefore by substituting eq.(2.20) in eq.(2.19) and by simplifying the equation we obtain

$$\frac{dA}{dz} = \frac{3}{2n\epsilon_0} \frac{\omega}{c_0} \chi_{im}^{(3)} A(z) |A(z)|^2 \quad (2.21)$$

In previous section we assumed that intensity of light is

$$I = \frac{|E(\omega)|^2}{2\eta} = \frac{|A(z)|^2}{2\eta} = \frac{A(z)A^*(z)}{2\eta} \quad (2.22)$$

where

$$\eta = \sqrt{\frac{\mu}{\epsilon}} = \sqrt{\frac{\mu_r \mu_0}{\epsilon_r \epsilon_0}} = \frac{\sqrt{\frac{\mu_0}{\epsilon_0}}}{\sqrt{\epsilon_r}} = \frac{\eta_0}{n}$$

By using the intensity formula we find

$$\frac{dI}{dz} = \frac{1}{2\eta} \left( A(z) \frac{dA^*(z)}{dz} + A^*(z) \frac{dA(z)}{dz} \right) = \frac{6\eta_0}{n^2 \epsilon_0} \chi_{im}^{(3)} \frac{\omega}{c_0} I^2 \quad (2.23)$$

The TPA coefficient is described as

$$\beta = \frac{1}{I^2} \frac{dI}{dz} \quad (2.24)$$

By using this definition  $\beta$  is

$$\beta = \frac{6\eta_0}{n^2 \epsilon_0} \chi_{im}^{(3)} \frac{\omega}{c_0} \quad (2.25)$$

where  $\eta_0$  is the impedance of the free space,  $n$  is the refractive index and  $c_0$  is the speed of light in free space.

Typical values for two photon coefficients are given in table 2.2

<i>Material</i>	<i><math>\beta</math> (cm / W)</i>
Fused Silica	$\sim 2 \times 10^{-11}$
Crystalline Quartz	$(1.2 \pm 0.2) \times 10^{-11}$
Sapphire	$(9.4 \pm 1.2) \times 10^{-11}$

Barium Borate Crystal	$(47 \pm 5) \times 10^{-11} \sim (68 \pm 6) \times 10^{-11}$
Liquids ( water, heavy water, ethanol, methanol, hexane, cyclohexane,1,2-dichloroethane )	$(34 \pm 3) \times 10^{-11} \sim (95 \pm 11) \times 10^{-11}$

**Tablo 2.2** Two Photon Absorption Coefficients

## 2.4 Four Wave Mixing

Four-wave mixing is another essential third order nonlinear effect and this effect will be used to generate and analyze the transient grating in the proposed switching node. The effect of four wave mixing can be understood by considering the response of the nonlinear medium to an optical field that consists of plane waves of frequencies  $\omega_1$ ,  $\omega_2$  and  $\omega_3$

$$E(t) = \text{Re} \left\{ E(\omega_1)e^{j\omega_1 t} + E(\omega_2)e^{j\omega_2 t} + E(\omega_3)e^{j\omega_3 t} \right\} \quad (2.26)$$

it is easy to write total electric field as

$$E(t) = \sum_{q=\pm 1, \pm 2, \pm 3} \frac{1}{2} E(\omega_q) e^{j\omega_q t} \quad (2.28)$$

where electric fields are assumed to be real;  $\omega_{-q} = \omega_q$  and  $E(-\omega_q) = E^*(\omega_q)$ . By placing this value into eq. (2.4), we obtain

$$P_1^{(3)}(t) = \frac{1}{2} \chi^{(3)} \sum_{q,r,l=\pm 1, \pm 2, \pm 3} E(\omega_q) E(\omega_r) E(\omega_l) e^{i(\omega_q + \omega_r + \omega_l)t} \quad (2.29)$$

The resulting polarization density consists of 44 different frequency components. Some of these frequencies are

$\omega_1, \omega_2, \omega_3$

$3\omega_1, 3\omega_2, 3\omega_3$

$\omega_1 + \omega_2 - \omega_3, \omega_1 - \omega_2 + \omega_3, -\omega_1 + \omega_2 + \omega_3, \omega_1 + \omega_2 + \omega_3$

$2\omega_1 \pm \omega_2, 2\omega_1 \pm \omega_3, 2\omega_2 \pm \omega_1, 2\omega_2 \pm \omega_3, 2\omega_3 \pm \omega_1, 2\omega_3 \pm \omega_2$

and etc.

These values are also the frequencies of a generated fourth wave due to polarization density behavior as source in nonlinear medium, previously described. Let us assume that we choose a component with frequency  $\omega_4 = \omega_1 + \omega_2 - \omega_3$ . In other word, we preferred the density that have argument  $\omega_1 + \omega_2 - \omega_3$

$$P_1^{(3)}(\omega_1 + \omega_2 - \omega_3) = 6\chi^{(3)}E(\omega_1)E(\omega_2)E^*(\omega_3) \quad (2.30)$$

When we put this component into Maxwell equations, it can be considered that four waves of frequencies  $w_1, w_2, w_3$  and  $w_4$  are mixed by the medium if

$$\omega_4 = \omega_1 + \omega_2 - \omega_3 \quad (2.31)$$

This assumption is the basic of the frequency matching condition

$$\omega_4 + \omega_3 = \omega_1 + \omega_2 \quad (2.32)$$

and phase matching condition

$$k_4 + k_3 = k_1 + k_2 \quad (2.33)$$

that must be satisfied in order a new wave with wave vector  $k_4 = k_1 + k_2 - k_3$  to be generated.

When the FWM is regarded as a quantum optical process, it can be interpreted as combination of photon photon of frequency  $w_1$  with a photon of frequency  $w_2$  to produce photons of frequencies  $w_3$  and  $w_4$ .

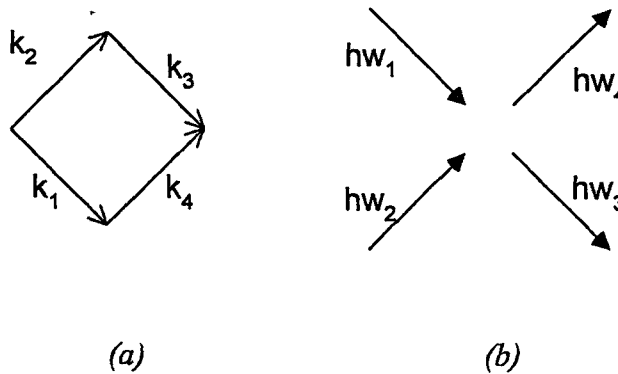


**Figure 2.2** Four wave mixing process

a) Phase matching condition b) FWM as photon interaction

# CHAPTER 3

## OPTICAL WAVEGUIDES ANALYZES TECHNIQUES AND GRATING ASSISTED COUPLERS

The main issue of this chapter is to investigate the techniques for transferring the light from one waveguide to another. The method proposed here depends on formation of a transient grating in the cladding region of the waveguide by interfering two Gaussian beams and then deflect the mode outside of this waveguide. To understand the mechanism of this structure, some basic knowledges about propagating of light inside the waveguide and about mathematical approaches to corrugated waveguide problem will be reminded first.

### 3.1 Propagation of Light in Waveguides

In order to prevent losses, carried energy have to be confined in the core of the waveguide. Thus, light has to undergo Total Internal Reflection. In fact, even the light is confined in the core, some amount of radiation extends into the cladding region. If the evanescent field is strong, so that it extends to the other side boundary, some amount of energy may radiate. This phenomenon is known as Frustrated Total Internal Reflection

#### 3.1.1 Ray approach: Total Internal Reflection and Frustrated Internal Reflection

The optimum way of guiding light without loss is total internal reflection that is illustrated in Figure 3.1

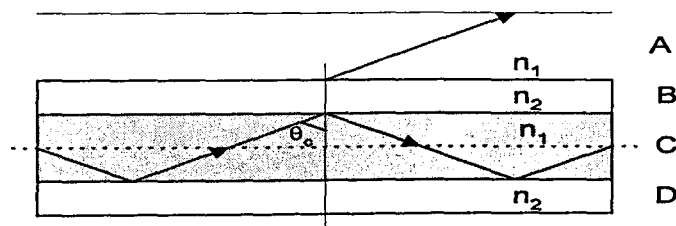


Figure 3.1 Total and Frustrated Internal Reflection

In this approach, it is assumed that all of the light is reflected if the incidence angle  $\theta$  is greater than the critical angle  $\theta_c$ , which is defined as follows by using Snell's law

$$\theta_c = \sin^{-1} \frac{n_2}{n_1} \quad (3.1)$$

It is very crucial to note that total internal reflection ( TIR ) produces propagating evanescent field in core cladding boundary (BC boundary) on the cladding side (B). This fundamental property will be used in analyzing the transient grating in the switching node. However, if the evanescent wave extends into the BA boundary, energy may flow into region A. This is known as Frustrated Total Internal Reflection (FTIR ) and is widely used in beamsplitters[S.O Kasap]. The energy transmitted in A carry some of the light intensity and the power of reflected beam is reduced.

### 3.1.2 Wave Approach : Waveguide Modes in a Slab Waveguide

The ray optics approach does not give a satisfactory information about a number of effects that occur during light guiding. Thus, wave approach is mandatory to explain the nature of light propagation in waveguides.

Consider a monochromatic wave of propagation constant  $\beta$  in z-direction, wavenumber

$k = nk_0$  and velocity  $c = \frac{c_0}{n}$ , where n is the refractive index of the medium. This wave

can be written in following form(Yariv 1997)

$$E(\mathbf{r},t) = E(x, y)e^{j(\omega t - \beta z)} \quad (3.2)$$

If this field is a mode of the dielectric waveguide shown in Figure 3.1, it must satisfy the wave equation

$$\nabla^2 E(\mathbf{r}) + k_0^2 n^2(\mathbf{r})E(\mathbf{r}) = 0 \quad (3.3)$$

If we assume that electric field have only x component, then wave equation can be written in the following form

$$\frac{\partial^2}{\partial x^2} E(x, y) + [k_0^2 n^2(\mathbf{r}) - \beta^2]E(x, y) = 0 \quad (3.4)$$



This equation can be separately writing for regions 1, 2 and 3

$$\text{Region 1} \quad \frac{\partial^2}{\partial x^2} E(x, y) + [k_0^2 n_1^2 - \beta^2] E(x, y) = 0 \quad (3.5a)$$

$$\text{Region 2} \quad \frac{\partial^2}{\partial x^2} E(x, y) + [k_0^2 n_2^2 - \beta^2] E(x, y) = 0 \quad (3.5b)$$

$$\text{Region 3} \quad \frac{\partial^2}{\partial x^2} E(x, y) + [k_0^2 n_3^2 - \beta^2] E(x, y) = 0 \quad (3.5c)$$

Let us assume that  $n_2 > n_3 > n_1$ . We know that propagation constant  $\beta$  can give an opinion about the nature of the solution. This situation is illustrated in Figure 3.2 .

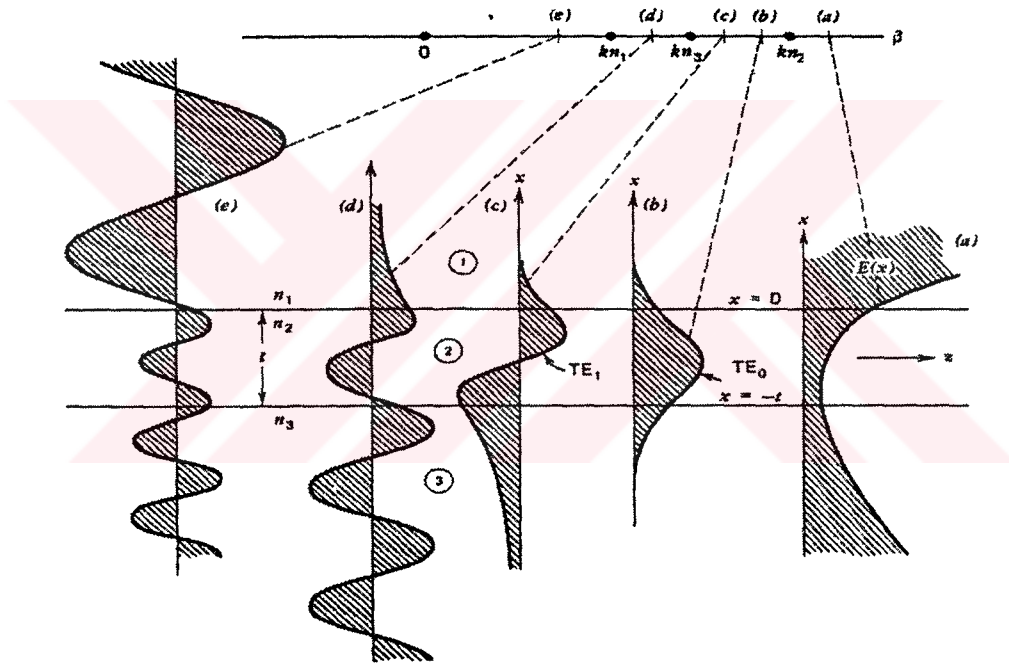


**Figure 3.2** The Field Distributions Corresponding To The Different Value Of  $\beta$

For  $\beta > k_0 n_2$ ,  $E(x)$  is exponential in all three regions 1,2,3 as shown in Figure 3.2a. This is not a physically realizable solution, thus we may decline the existence of such a wave.

For  $k_0 n_3 < \beta < k_0 n_2$ , the solution  $E(x)$  is sinusoidal in region 2 and exponential in 1 and 3. The solutions are shown in in Figure 3.2b and 3.2c, where most of energy of the wave is carried in region 2, that refers to the guiding mode. As a result, it may be

concluded that the mode is guiding only if  $k_0 n_1, k_0 n_3 < \beta < k_0 n_2$  that leads to logical consequence  $n_2 > n_1, n_3$ .

The situation  $k_0 n_1 < \beta < k_0 n_3$  refers to the Figure 3.2d, where  $E(x)$  is exponential in region 1 and sinusoidal in regions 2 and 3. These are the substrate radiation modes. However, for  $0 < \beta < k_0 n_1$  the solution becomes sinusoidal for all three regions and these are the modes called radiation modes of the waveguide and this is shown in Figure 3.2e.

It is important to note that  $\beta$  is a continuous variable in regimes (d) and (e), whereas it is in discrete form in  $k_0 n_3 < \beta < k_0 n_2$  situation. The number of modes depends on the width of the waveguide, the frequency and the refractive indices  $n_1, n_2$  and  $n_3$ .

### 3.2 Perturbation Analysis of Corrugated Periodic Waveguides

Small periodic perturbations (gratings) in a guided wave devices have broad applications in optoelectronics. Grating devices have been widely used as optical couplers, wavelength selective filters, wavelength division multiplexers, dispersion compensators and Distributed Feedback Lasers. Many of these devices are being analyzed by Coupled Mode Theory, Rigorous Full Wave Analyses, Transfer Matrix Method and Floquet theory. Coupled wave method, that uses a mode matching technique to determine power coupling, is the standard grating analysing method and it is also the approach that we used in analysing the proposed switch. Coupled wave method regards grating as a small perturbation that couples only one forward and one backward propagating mode of the waveguide, while leaving other modes unexcited. This model is inaccurate if the grating perturbation is strong or one of the modes is leaky.

Let us consider the coupling of forward to backward modes that is caused by the perturbation ( refractive index change ) in one side of the waveguide. We know that wave equation can be written as follows (Yariv 1997)

$$\nabla^2 E(r, t) - \mu \epsilon \frac{\partial^2 E(r, t)}{\partial t^2} = \mu \frac{\partial^2 P(r, t)}{\partial t^2} \quad (3.6)$$

where polarization density is

$$P(\mathbf{r}, t) = P_0(\mathbf{r}, t) + P_{\text{pert}}(\mathbf{r}, t) \quad (3.7)$$

$P_0(\mathbf{r}, t)$  is the polarization induced by  $E(\mathbf{r}, t)$  in the unperturbed waveguide and can be defined in the following form

$$P_0(\mathbf{r}, t) = (\epsilon(\mathbf{r}) - \epsilon_0)E(\mathbf{r}, t) \quad (3.8)$$

where  $\epsilon(\mathbf{r})$  is the dielectric constant of the unperturbed waveguide. The perturbation polarization  $P_{\text{pert}}(\mathbf{r}, t)$  refers to deviation of the unperturbed waveguide polarization density. By using all of this definition, the wave equation can be written in the following form

$$\nabla^2 E(\mathbf{r}, t) - \mu\epsilon(\mathbf{r}) \frac{\partial^2 E(\mathbf{r}, t)}{\partial t^2} = \mu \frac{\partial^2 P_{\text{pert}}(\mathbf{r}, t)}{\partial t^2} \quad (3.9)$$

We may assume that electric field is changing only with respect to  $x$ , then the total field confined in the waveguide can be written as the superposition of all field, that is

$$E(\mathbf{r}, t) = \frac{1}{2} \sum_m A_m(z) E^m(x) e^{j(\omega t - \beta_m z)} + \text{c.c} \quad (3.10)$$

where  $m$  is number of the discrete mode that satisfy wave equation

$$\left( \frac{\partial}{\partial x^2} - \beta_m^2 \right) E^{(m)}(\mathbf{r}) + w^2 \mu\epsilon(\mathbf{r}) E^m(\mathbf{r}) = 0 \quad (3.11)$$

where  $\epsilon(\mathbf{r}) = \epsilon_0 n^2(\mathbf{r})$

Combining 3.9 and 3.10 gives

$$\begin{aligned}
& e^{j\omega t} \sum_m \left[ \frac{A_m}{2} \left( -\beta_m^2 E^{(m)} + \frac{\partial^2 E^{(m)}}{\partial x^2} + \omega^2 \mu \epsilon(\mathbf{r}) E^{(m)} \right) e^{-j\beta_m z} + \right. \\
& \left. + \frac{1}{2} \left( -2j\beta_m \frac{dA_m}{dz} + \frac{d^2 A}{dz^2} \right) E^{(m)} e^{-j\beta_m z} \right] + \text{c.c} \\
& = \mu \frac{\partial^2}{\partial t^2} P_{\text{pert}}(\mathbf{r}, t)
\end{aligned} \tag{3.12}$$

According to eq.(3.12), the sum  $\left[ -\beta_m^2 E^{(m)} + \frac{\partial^2 E^{(m)}}{\partial x^2} + \omega^2 \mu \epsilon(\mathbf{r}) E^{(m)} \right]$  is equal to zero.

Furthermore, by assuming slowly varying approximation (SVA)  $\left| \frac{d^2 A_m}{dz^2} \right| \ll \beta_m \left| \frac{dA_m}{dz} \right|$

and using eq.(3.12) we obtain

$$\sum_m -j\beta_m \frac{dA_m}{dz} E^{(m)} e^{j(\omega t - \beta_m z)} + \text{c.c} = \mu \frac{\partial^2}{\partial t^2} P_{\text{pert}}(\mathbf{r}, t) \tag{3.13}$$

When we take the product of 3.13 with  $E^{(s)}(x)$ , integrate from  $-\infty$  to  $\infty$  and use the mode orthogonality property

$$\int_{-\infty}^{\infty} E^{(l)}(x) E^{(m)}(x) dx = \frac{2\omega\mu}{\beta_m} \delta_{l,m}$$

we obtain

$$\begin{aligned}
& \frac{dA_s^{(-)}}{dz} e^{j(\omega t + \beta_s z)} - \frac{dA_s^{(+)}}{dz} e^{j(\omega t - \beta_s z)} - \text{c.c} = \\
& = -\frac{j}{2\omega} \frac{\partial^2}{\partial t^2} \int_{-\infty}^{\infty} [P_{\text{pert}}(\mathbf{r}, t)] E^{(s)}(x) dx
\end{aligned} \tag{3.14}$$

The left side of the eq.(3.14) consists of two terms; one for wave travelling in the (-z) direction and labeled with (-) and one term for wave travelling in the (+z) direction and indicated with (+).

In order to clarify the eq.(3.14), consider a dielectric waveguide with a corrugation in one side as shown in Figure 3.3.

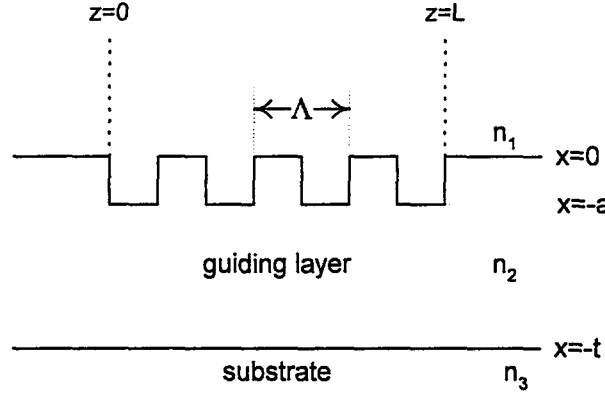


**Figure 3.3** A corrugated periodic waveguide

Let us assume that perturbation is due to a periodic grating, where refractive index variation is described by the dielectric constant, which can be defined as following

$$\varepsilon'(\mathbf{r}) = \varepsilon(\mathbf{r}) + \Delta\varepsilon(\mathbf{r}) \quad (3.15)$$

where  $\Delta\varepsilon(\mathbf{r}) \equiv \varepsilon_0 \Delta n^2(\mathbf{r})$ . The perturbation polarization density can be written as

$$\mathbf{P}_{\text{pert}}(\mathbf{r}, t) = \Delta\varepsilon(\mathbf{r})\mathbf{E}(\mathbf{r}, t) = \Delta n^2(\mathbf{r})\varepsilon_0\mathbf{E}(\mathbf{r}, t) \quad (3.16)$$

Substituting eq.(3.10) in eq.(3.16) leads to

$$\mathbf{P}_{\text{pert}}(\mathbf{r}, t) = \frac{\Delta n^2(\mathbf{r})\varepsilon_0}{2} \sum_m A_m E^m(\mathbf{x}) e^{j(\omega t - \beta_m z)} + \text{c.c} \quad (3.17)$$

By using this equation in eq.(3.14) gives

$$\begin{aligned} \frac{dA_s^{(-)}}{dz} e^{i(\omega t + \beta_s z)} - \frac{dA_s^{(+)}}{dz} e^{i(\omega t - \beta_s z)} - \text{c.c} = \\ = -\frac{j\varepsilon_0}{4\omega} \frac{\partial^2}{\partial t^2} \sum_m \left[ A_m \int_{-\infty}^{\infty} \Delta n^2(\mathbf{x}, z) E^m(\mathbf{x}) E^{(s)}(\mathbf{x}) dx e^{i(\omega t - \beta_m z)} + \text{c.c} \right] \end{aligned} \quad (3.18)$$

We may consider the right side of eq.(3.18) as a source wave term of the forward wave  $A_s^{(+)} e^{j(\omega t - \beta_s z)}$  and the backward wave  $A_s^{(-)} e^{j(\omega t + \beta_s z)}$  on the left side. In order for a wave to be driven by a source, both source wave and driven wave must have the same frequency so that the interaction does not average out to zero with distance of propagation  $z$ . For example, if it is desired that the forward wave  $A_s^+ e^{j(\omega t - \beta_s z)}$  be excited, it is necessary that at least one term on the right side of eq.(3.18), say the  $l$ th one, vary as  $e^{j(\omega t - \beta_s z)}$  with  $\beta \approx \beta_s$ . This situation is described by saying that the perturbation  $\Delta n^2(x, z)$  couples the forward (+) mode to the  $l$ th mode (Yariv 1997).

The permittivity function is periodical along  $z$  only in the grating region, that is refractive index change  $\Delta n^2(x, z)$  can be written according to Fourier series expansion as

$$\Delta n(x, z) = \Delta n(x) \sum_{q=-\infty}^{\infty} a_q e^{j\left(\frac{2q\pi}{\Lambda}\right)z} \quad (3.19)$$

where  $q$  denotes the  $q$ th harmonic and  $\Lambda$  is the period of the square wave grating.

Wave coupling is the resonant process and the grating period is an important parameter to obtain high efficient power transfer between the modes and this efficiency strongly depends on the grating index change. The resonance condition is

$$\frac{2l\pi}{\Lambda} - \beta_s \approx \beta_s$$

so that the grating period is so chosen that  $\frac{l\pi}{\Lambda} \approx \beta_s$ . From resonance condition equation, it is obvious that conventional coupled mode theory determines the grating period in an approximated form.

By assuming the forward wave as the source of the backward wave ( $m=s$ ) and combining eq.(3.19) with eq.(3.18) we can write

$$\frac{dA_s^{(-)}}{dz} = \frac{j\omega\epsilon_0}{4} A_s^{(+)} \int_{-\infty}^{\infty} \Delta n^2(x) [E^{(s)}(x)]^2 dx a_l e^{j\left[\left(\frac{2l\pi}{\Lambda}\right) - 2\beta_s\right]z} \quad (3.20)$$

Thus, by considering eq.(3.20), the general form of the coupling between the backward wave  $A_s^{(-)}$  and the forward wave  $A_s^{(+)}$  by the grating can be described as

$$\frac{dA_s^{(-)}}{dz} = \kappa A_s^{(+)} e^{-j2(\Delta\beta)z} \quad (3.21)$$

and similarly

$$\frac{dA_s^{(+)}}{dz} = \kappa^* A_s^{(-)} e^{j2(\Delta\beta)z} \quad (3.22)$$

where

$$\kappa = \frac{jw\epsilon_0 a_1}{4} \int_{-\infty}^{\infty} \Delta n^2(x) [E^{(s)}(x)] dx \quad (3.23)$$

and

$$\Delta\beta \equiv \beta_s - \frac{l\pi}{\Lambda} \equiv \beta_s - \beta_0 \quad (3.24)$$

Let us assume that  $A_s^{(-)} \equiv A$ ,  $A_s^{(+)} \equiv B$  and substitute them in eq.(3.21) and (3.22)

$$\frac{dA}{dz} = \kappa_{ab} B e^{-j2(\Delta\beta)z} \quad (3.25a)$$

$$\frac{dB}{dz} = \kappa_{ab}^* A e^{j2(\Delta\beta)z} \quad (3.25b)$$

Consider a waveguide with a perturbation of length  $L$  as that in Figure 3.3. Let us suppose that the forward wave with an amplitude  $B(0)$  is entering on the corrugated region and the amplitude of the backward wave at  $z=L$ ,  $A(L) = 0$ . Also, assume that total power is conserved, that is

$$\frac{d}{dz} (|A(z)|^2 + |B(z)|^2) = 0 \quad (3.26)$$

By using all of this condition, one can obtain the following equations

↓  
arka sayfaya

$$A(z)e^{j\beta z} = B(0) \frac{jk_{ab} e^{j\beta_0 z}}{-\Delta\beta \sinh SL + jS \cosh SL} \sinh[S(z-L)] \quad (3.27a)$$

$$B(z)e^{-j\beta z} = B(0) \frac{e^{-j\beta_0 z}}{-\Delta\beta \sinh SL + jS \cosh SL} \times \{\Delta\beta \sinh[S(z-L)] + jS \cosh[S(z-L)]\} \quad (3.27b)$$

where

$$S = \sqrt{\kappa^2 - \Delta\beta^2} \quad (3.28)$$

$$\kappa \equiv |\kappa_{ab}| \quad (3.29)$$

Under the matching condition  $\Delta\beta = 0$ , we obtain

$$A(z) = B(0) \frac{\kappa_{ab} \sinh[\kappa(z-L)]}{\kappa \cosh \kappa L} \quad (3.30a)$$

$$B(z) = B(0) \frac{\kappa_{ab} \cosh[\kappa(z-L)]}{\kappa \cosh \kappa L} \quad (3.30b)$$

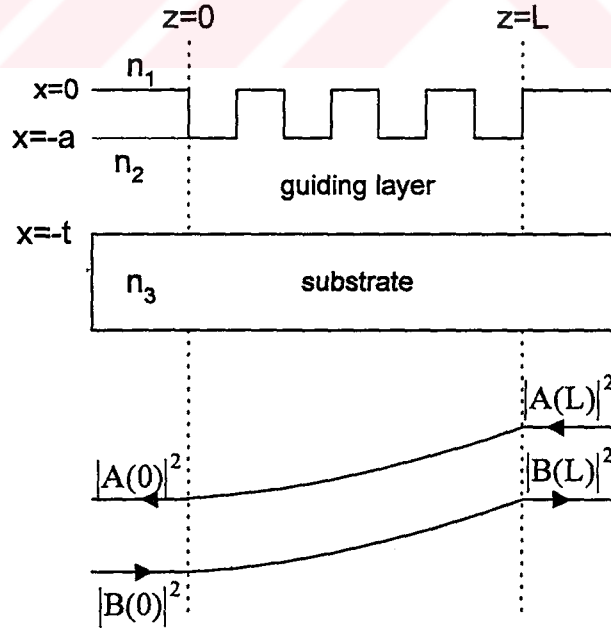


**Figure 3.4** The incident and reflected intensities in the corrugated section



From eq.3.30 it is obvious that coupling coefficient  $\kappa$  is the key factor to find the exchanged power. Nevertheless, eq.(3.23) shows the standard technique to determine  $\kappa$ , where the grating perturbation and the unperturbed mode is integrated to find the coupling coefficient. However, this technique works well for weak perturbations, but for the strong perturbations the choice of the unperturbed waveguide geometry is crucial and have a great influence over the coupling coefficient. In order to discard this problem in Distributed Feedback Lasers, the ray optics method was proposed to find the coupling coefficient in coupled mode equations(Luo and Zory 1990).

### 3.3 Distributed Feedback Laser Approach

The idea of the distributed feedback lasers is to put a grating(corrugation) into cavity of the laser. Here, grating refers to a periodic variation in refractive index of the gain region, along its length. The presence of the grating causes small reflections at each perturbation and when the period of the corrugation is a multiple of the incident light wavelength, constructive interference between reflections occur and the proportion of the light is reflected. Other wavelengths destructively interfere, therefore they can not be reflected.

The reflection of forward waves into backward waves, and vice versa, can be defined by using the coupled mode equations, that we derived in previous section. Luo and Zory derived an analytical solution for the coupling coefficients for both weak and strong coupling DFB waveguide structures by using the ray-optics method. In this method, the unperturbed waveguide geometry was chosen arbitrarily and assumed that the first order mode of diffraction is dominant and all higher modes are neglected. This is a reasonable approach, because laterly we will show that by rearranging the grating structure, the first diffraction order could be approximated as dominant.

Figure 3.5 is a grating waveguide structure, that can be assumed as a rough approximation to a transient grating, analysed in this thesis.

The waveguide consists of cladding, guiding and substrate layers that have refractive indices of  $n_a$ ,  $n_b$ ,  $n_c$ , respectively. The grating is on the cladding – guiding layer boundary and its depth is defined as  $d$ .

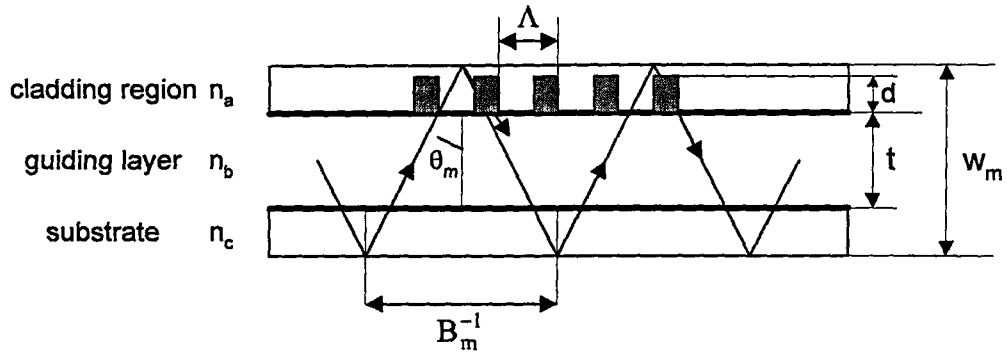


**Figure 3.5** Typical Grating Waveguide Device

The coupling coefficient of the corrugated waveguide can be written as following(Luo and Zory 1994).

$$\kappa = \sqrt{\eta} B_m \quad (3.31)$$

where  $B_m$  is bounce rate for mode  $m$  and  $\eta$  is the diffraction efficiency of the mode propagating at angle  $\theta_m$ .

The bounce rate  $B_m$  is defined by the following expression

$$B_m = (2w_m \tan \theta_m)^{-1} \quad (3.32)$$

where  $w_m$  is the effective waveguide thickness.

The effective waveguide thickness for the  $m$ th mode is (PARK S. et al. 2001)

$$w_m = t + \frac{1}{q_m} + \frac{1}{p_m} \quad (3.33)$$

where

$$q_m = k_0 (n_m^2 - n_a^2)^{\frac{1}{2}} \quad (3.34)$$

$$p_m = k_0 (n_m^2 - n_c^2)^{\frac{1}{2}} \quad (3.35)$$

$k_0$  is the wavenumber of light in vacuum and  $n_m = n_b \sin \theta_m$  is the effective index of

the guiding layer for  $m$ th mode.

Although, it is possible to find an analytic expression for the diffraction efficiency, in our calculations we will obtain it from the computer simulation results. Therefore, I will not derive any formula for diffraction efficiency here.

### 3.4 Photonic Crystal

From the analyzes carried out in sections 3.2 and 3.3, it can be understood that the main purpose of using a grating structure is to control and manipulate the light. Another solution to this problem is employing a photonic crystal instead of a grating.

Photonic crystals are periodic structure that have photonic band gaps. These gaps are ranges of frequency in which light can not propagate through the structure. Figure 3.6 illustrates one dimensional photonic crystal.

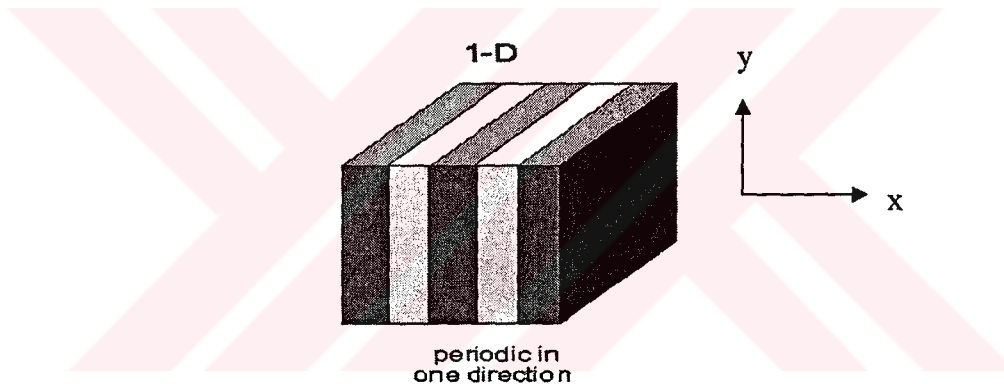


**Figure 3.6** One Dimensional Photonic Crystal

Let us suppose that an electromagnetic wave, perpendicular to the surface, is incident on the periodic structure shown in Figure 3.6. We assume that wave is travelling in the  $x$  direction and polarized along  $y$  axis. Electric field  $E(x,t)$  must satisfy the wave equation, which in a nonmagnetic material can be written as (Sakoda 2001)

$$\frac{c^2}{\epsilon_r(x)} \frac{\partial^2 E}{\partial x^2} - \frac{\partial^2 E}{\partial t^2} = 0 \quad (3.36)$$

where  $\epsilon_r(x)$  is the relative dielectric constant of the crystal and it is position dependent due to the nature of the crystal. Dielectric constant is a periodic function and it can be written as

$$\varepsilon_r(x+a) = \varepsilon_r(x) \quad (3.37)$$

$\varepsilon_r^{-1}(x)$  is also periodic and can be written as the sum of Fourier components

$$\varepsilon_r^{-1}(x) = \sum_{m=-\infty}^{\infty} \kappa_m e^{j\left(\frac{2\pi m}{a}x\right)} \quad (3.38)$$

where  $\kappa_m$  are Fourier coefficients.

In order to define the electric field in the crystals, we may use the Floquet-Bloch for the nature of an electromagnetic wave travelling in a medium with periodic layers. This theorem states that electric and magnetic fields in periodic medium also have periodic forms with the wavevector  $k$ , called Bloch wave vector. Thus, electric field can be expressed in a general form as following

$$E(x, t) \equiv E_k(x, t) = u_k(x) e^{j(kx - \omega_k t)} \quad (3.39)$$

where  $k$  is the Bloch wavenumber and  $\omega_k$  express the angular frequency that depends on Bloch wavenumber.  $u_k(x)$  is a periodic function such that

$$u_k(x+a) = u_k(x) \quad (3.40)$$

Hence,  $u_k(x)$  can be expanded in a Fourier series and electric field can be written in following form

$$E_k(x, t) = \sum_{m=-\infty}^{\infty} E_m e^{j\left(k + \frac{2\pi m}{a}\right)x - i\omega_k t} \quad (3.41)$$

where  $E_m$  are the Fourier coefficients.

Let us assume that components with  $m = 0$  and  $m = \pm 1$  are dominant, then we rewrite eq.(3.38)

$$\varepsilon_r^{-1}(x) \approx \kappa_0 + \kappa_1 e^{j\left(\frac{2\pi}{a}x\right)} + \kappa_{-1} e^{j\left(-\frac{2\pi}{a}x\right)} \quad (3.42)$$

Combining eq.(3.42), eq.(3.41) and eq.(3.36) leads to

$$\begin{aligned} \kappa_1 \left[ k + \frac{2(m-1)\pi}{a} \right]^2 E_{m-1} + \kappa_{-1} \left[ k + \frac{2(m+1)\pi}{a} \right]^2 E_{m+1} &\approx \\ &\approx \left[ \frac{\omega_k^2}{c^2} - \kappa_0 \left( k + \frac{2m\pi}{a} \right)^2 \right] E_m \end{aligned} \quad (3.43)$$

For  $m = 0$ ,

$$E_0 \approx \frac{c^2}{\omega_k^2 - \kappa_0 c^2 k^2} \left[ \kappa_1 \left( k - \frac{2\pi}{a} \right)^2 E_{-1} + \kappa_{-1} \left( k + \frac{2\pi}{a} \right)^2 E_1 \right] \quad (3.44)$$

For  $m = -1$ ,

$$E_{-1} \approx \frac{c^2}{\omega_k^2 - \kappa_0 c^2 \left( k - \frac{2\pi}{a} \right)^2} \left[ \kappa_1 \left( k - \frac{4\pi}{a} \right)^2 E_{-2} + \kappa_{-1} k^2 E_0 \right] \quad (3.45)$$

If  $k \approx \frac{\pi}{a}$  and  $\omega_k^2 \approx \kappa_0 c^2 k^2$ , then  $E_0$  and  $E_{-1}$  are dominant and eq.(3.44) and eq.(3.45) can be written as two coupled equations

$$\left( \omega_k^2 - \kappa_0 c^2 k^2 \right) E_0 - \kappa_1 \left( k - \frac{2\pi}{a} \right)^2 E_{-1} = 0 \quad (3.46)$$

$$-\kappa_{-1} c^2 k^2 E_0 + \left( \omega_k^2 - \kappa_0 c^2 \left( k - \frac{2\pi}{a} \right)^2 \right) E_{-1} = 0 \quad (3.47)$$

In order to find the frequency range, where there exist no field, we must look for the nontrivial solution of the above equations (3.46) and (3.47), that is when the determinant of coefficients is zero:

$$\begin{vmatrix} \left( \omega_k^2 - \kappa_0 c^2 k^2 \right) & -\kappa_1 \left( k - \frac{2\pi}{a} \right)^2 \\ -\kappa_{-1} c^2 k^2 & \omega_k^2 - \kappa_0 c^2 \left( k - \frac{2\pi}{a} \right)^2 \end{vmatrix} = 0 \quad (3.48)$$

If we introduce  $h = k - \frac{\pi}{a}$ , the solution  $|h| \ll \frac{\pi}{a}$  is

$$\omega_{\pm} \approx \frac{\pi c}{a} \sqrt{\kappa_0 \pm |\kappa_1|} \pm \frac{ac}{\pi |\kappa_1|} \left( \kappa_0^2 - \frac{|\kappa_1|^2}{2} \right) \hbar^2 \quad (3.49)$$

This indicates that there is no mode in the interval

$$\frac{\pi c}{a} \sqrt{\kappa_0 - |\kappa_1|} < \omega < \frac{\pi c}{a} \sqrt{\kappa_0 + |\kappa_1|} \quad (3.50)$$

This situation is illustrated better in Figure 3.7

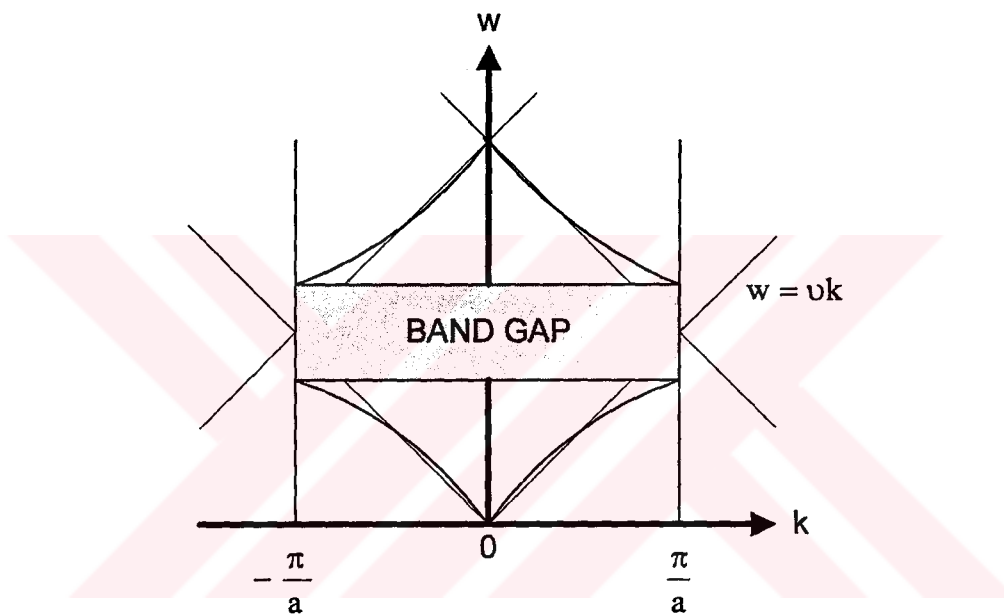


**Figure 3.7** Dispersion Relation For a 1D Photonic Crystal

# CHAPTER 4

## ALL OPTICAL SWITCHING NODE

### 4.1 Introduction

An optical packet switch is a device which is used for distributing signals from input ports into output ports. It may consist of a few components or it may contain complex controlling blocks, delay line buffers, filters, wavelength converters and simple switches. In this chapter we will consider a switch fabric concept and after that we will introduce an all optical switching node that relies on a transient grating mechanism and coupling structure.

The structure of a single line switch fabric is shown in figure 4.1. This fabric consists of a number of switching nodes which are active only in the existence of a grating pattern. However, in the lack of grating the information carrying optical signal is transmitted to the next node without any manipulation.

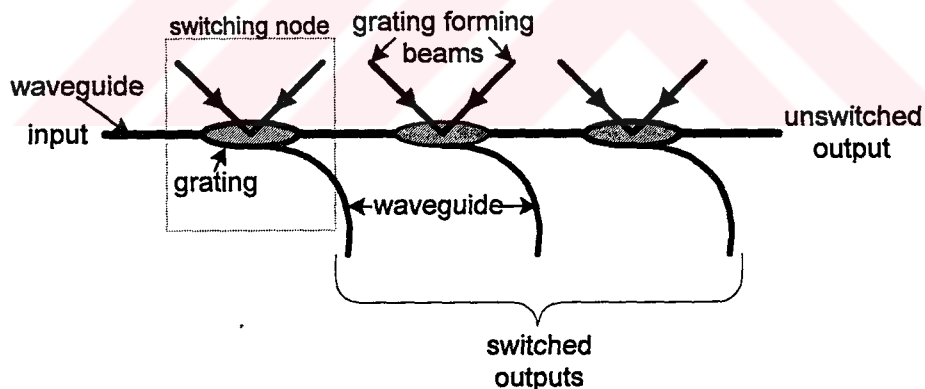


**Figure 4.1** Nodes in Single Line All Optical Switch Fabric

When there is a packet to be switched or routed at the input of the switch fabric, the relevant switching node is activated by forming the transient grating. This grating is formed by interference of two Gaussian beams, that travel at a very small angle with respect to normal of the cladding – guiding medium boundary of the waveguide. The mode travelling in the guiding layer interacts with the generated transient grating and

this leads to the well known Four Wave Mixing process in the third order nonlinear ( $\chi^{(3)}$ ) material. This interaction destroys the lateral resonance or total internal reflection. In order to complete the switching procedure, the destroyed mode have to be transfered to another waveguide. Placing periodic grating structure between two waveguides is one of the most common way to transfer the energy between the waveguides. As far as the best efficiency known is obtained in (Masanovic et. al.2003) and it is about 90% for non-transient grating, while the other reported coupling efficiency is about 40% in (Butler et. al 1998). It is obvious that all optical switching is a mode coupling process which occurs between two waveguides and its efficient implementation is the main issue of this chapter.

## 4.2 The Switching Node Model

In this work, two laser beams are interfered inside the cladding region of the waveguide to form a transient grating index. This structure is too close to the core-cladding boundary to destroy the guiding properties of the waveguide. In other words, transient grating changes the angle of reflectance of the guided light at this side of the waveguide. This problem might be studied by a number of techniques. First, four wave mixing (FWM) technique might be applied to the core-cladding boundary by considering the evanescent behavior of the waveguides mode that exist in the cladding region. In other method reflected waves from stationary grating may be used as that in many experimental works occurs when quasi stationary grating exist. In this case the grating might be considered as a perturbation. Another approach might be placing one dimensional photonic crystal with some forbidden band gap property in the cladding. In this structure, photonic crystal will not allow some of the waveguide modes to propagate, as explained in chapter 3.4.

The switching node, proposed in this thesis is shown in figure 4.2. In this structure, switching process occurs in two stages. In the first step, a transient grating is formed by interference of waves  $k_1$  and  $k_2$ . Hereafter, the propagating wave  $k_3$  interacts with the created grating that deflects the mode from total internal reflection. This is the consequence of the Four Wave Mixing, described previously in chapter 2 and shortly, we may assume that the effect of this process is a generation of new wave with wavevector  $k_4$ .



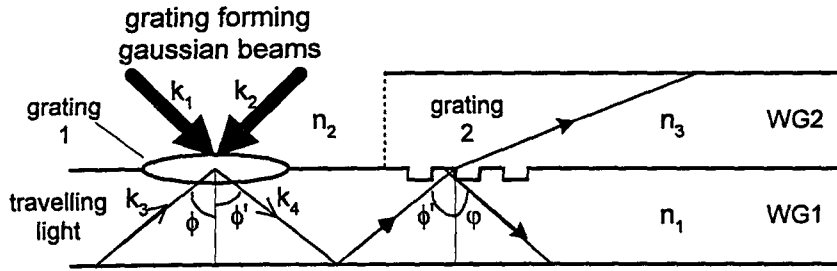


**Figure 4.2** The transient grating formation on the side of a waveguide and grating assisted directional coupler

The wave properties can be calculated regarding to the phase matching and frequency matching conditions of the FWM approach. In addition, the angle between  $k_4$  wavevector and the grating normal, that is  $\phi'$ , is an important parameter and it is needed for determining the coupling structure in the next stage. The second part is designed with an appropriate permanent grating for coupling maximum light energy from waveguide WG1 to waveguide WG2.

As a prerequisite, we would like to have grating forming laser that have different wavelength than the propagation light modes. Reflection from the permanent grating and FWM processes may be only differentiated due to grating strength and stationarity. This points needs to be investigated experimentally, too, as in our list of experimental work.

### 4.3 Deflection Angle Calculation

In order to clarify the transient grating and propagating mode interaction, consider the geometry shown in Figure 4.3. In this structure, two waves with wavevectors  $k_1, k_2$  are interfered in the cladding region of a waveguide to form a refractive index modulation (grating) and the propagating mode that have wavevector  $k_3$  is influenced by the modulated area.

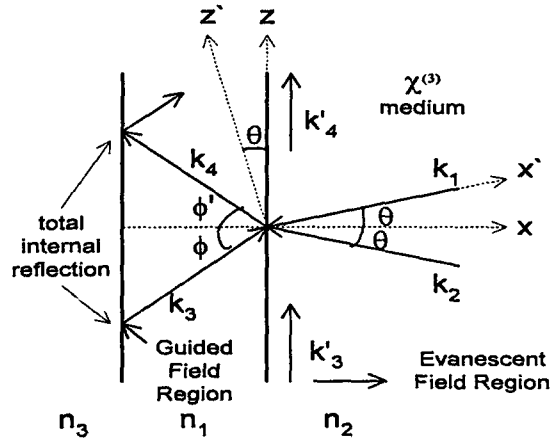


**Figure 4.3** FWM at the core – cladding boundary

This effect may be investigated by using the Four Wave Mixing process, that was explained in general in Chapter 2. Four Wave Mixing matching requirements were depicted in eq.(2.31) and eq.(2.32). According to the structure shown in Figure 4.3, the evanescent field with wavevector  $k'_3$  in cladding region interacts with the grating forming beams with wavevectors  $k_1$  and  $k_2$ . Thus, the matching conditions can be rewritten as

$$\omega_4 = \omega_1 - \omega_2 + \omega_3 \quad (4.1)$$

$$\vec{k}_4 = \vec{k}_1 - \vec{k}_2 + \vec{k}'_3 \quad (4.2)$$

where  $\vec{k}_1, \vec{k}_2, \vec{k}'_3, \vec{k}'_4$  are given as follows

$$\vec{k}_1 = -|k_1| \sin(\theta) \hat{z} - |k_1| \cos(\theta) \hat{x} \quad (4.3)$$

$$\vec{k}_2 = |k_2| \sin(\theta) \hat{z} - |k_2| \cos(\theta) \hat{x} \quad (4.4)$$

$$\vec{k}_3 = |k_3| \sin(\phi) \hat{z} + |k_3| \cos(\phi) \hat{x} \quad (4.5)$$

$$\vec{k}_4 = |k_4| \sin(\phi') \hat{z} - |k_4| \cos(\phi') \hat{x} \quad (4.6)$$

$$\vec{k}'_3 = |k_3| \sin(\phi) \hat{z} - j\alpha_1 \hat{x} \quad (4.7)$$

$$\vec{k}'_4 = |k_4| \sin(\phi') \hat{z} - j\alpha_2 \hat{x} \quad (4.8)$$

$$\alpha = \frac{2\pi}{\lambda} n_2 \sqrt{\frac{n_1^2}{n_2^2} \sin^2 \phi - 1} \quad (4.9)$$

where  $\alpha$  is the attenuation coefficient of the evanescent field in the cladding region (Saleh).

$$|k_1| = \frac{2\pi}{\lambda_0} n_2 \quad |k_2| = \frac{2\pi}{\lambda_0} n_2 \quad (4.10a)$$

$$|k_3| = \frac{2\pi}{\lambda} n_1 \quad |k_4| = \frac{2\pi}{\lambda} n_1 \quad (4.10b)$$

$$\omega = 2\pi\nu = 2\pi \frac{c_0}{\lambda n} \quad (4.11a)$$

$$\omega_1 = \omega_2 = 2\pi \frac{c_0}{\lambda_0 n_2} \quad (4.11b)$$

$$\omega_3 = \omega_4 = 2\pi \frac{c_0}{\lambda_0 n_2} \quad (4.11c)$$

In this equations  $\lambda_0$  is the wavelength of the grating forming beams, while  $\lambda$  is the wavelength of the guided light .

The importance of the matching equations (4.1) and (4.2) arises from the terms  $k'_3$  and  $k'_4$  which show that FWM process occurs in the cladding region close to the core-cladding boundary where the waveguide mode shows evanescent property.

After applying phase matching conditions, we obtain

$$|k_4| \sin(\phi') = -2 |k_1| \sin(\theta) + |k_3| \sin(\phi) \quad (4.12)$$

From eq.(4.11) it is obvious that  $|k_1| = |k_2|$  and  $|k_3| = |k_4|$ . In addition it can be assumed that the attenuation coefficients in the x direction are equal, that is  $\alpha_1 = \alpha_2$ . After some algebraic manipulation and using defined assumptions given above, following equation can be obtained easily

$$\frac{2\pi}{\lambda} n_1 \sin(\phi') = -2 \frac{2\pi}{\lambda_0} n_2 \sin(\theta) + \frac{2\pi}{\lambda} n_1 \sin(\phi) \quad (4.13)$$

From the eq. (4.13) it is evident that  $\phi'$  can be slightly different from  $\phi$  due to the designed grating.

The switching mechanism can be investigated either the modes are propagating when grating exist or vice versa. Let's consider the latter case, i.e assume that the switching occurs when grating is present. Otherwise the mode is propagating through the grating region without any deviation. If the mode exists and propagates in the core region, then evanescent field extension does exist in the cladding and this field interacts with the grating. In this situation reflection angle can be computed from eq. (4.13)

$$\sin \phi' = \sin \phi - \frac{n_2}{n_1} \frac{\lambda}{\lambda_0} 2 \sin \theta \quad (4.14)$$

According to this equation  $\theta$  and  $\lambda_0$  can be used as design parameters. Let's assume that the period of the grating in the z direction is defined by  $\Lambda$  for plane waves, where

$$\Lambda = \frac{\lambda_0}{2 n_2 \sin(\theta)} \quad (4.15)$$

then, from eq.(4.14) we can write reflection angle

$$\sin \phi' = \sin(\phi) - \frac{\lambda}{n_1} \frac{1}{\Lambda} \quad (4.16)$$

If grating exist, then the internal reflection angle is different from incident angle as defined in eq.(4.16). This situation can be best explained by an example of normal propagating modes in slab waveguide with refractive indices of  $n_1 = 1.4801$  and  $n_2 = 1.465$  for the configuration shown in figure 4.3. If the propagation constant along z direction is denoted as  $\beta$ , then

$$\beta = n_1 k_0 \sin(\phi) \quad (4.17)$$

By using the Snell's law, the critical incident angle can be shown by

$$\phi_c = \sin^{-1} \frac{n_2}{n_1} \quad (4.18)$$

With the values given above critical angle is  $\phi_c = 81.8^\circ$ .

Let us consider a mode which has incident angle  $\phi = 81.8^\circ$  and wavelength  $\lambda = 1.55\mu\text{m}$ . For the values given above, propagation constant  $\beta$  is equal to  $5.94 \times 10^6$  rad/m and the mode can be diffracted out from the waveguide by choosing  $\phi' < \phi_c$ . If the incident angle of grating forming plane waves is  $\theta = 1^\circ$  with wavelength  $\lambda_0 = 1\mu\text{m}$ , then grating period  $\Lambda$  is equal to  $19.55\mu\text{m}$ . For these values, reflection angle  $\phi'$  of beam diffracted from grating is  $69.42^\circ$ . Therefore, the permanent grating in the second stage should be designed to couple the mode with angle  $69.42^\circ$  as high efficient as possible.

#### 4.4 Three Dimensional Grating Formation

In the previous section we carried out a simple analysis by using ray optics approach to understand the grating effects on the propagating mode. In this analysis we assumed that the grating is a purely sinusoidal and found that it deflects the propagating mode from the total internal reflection. Now, let us assume that the grating is formed by interference of two Gaussian beams and analyze the influence of this type grating on the overall efficiency of the switching node.

##### 4.4.1 General Expression For a Gaussian Beam

A general expression for the complex amplitude  $U(\mathbf{r})$  of the Gaussian beam travelling in z-direction can be written as[Saleh]

$$U(\mathbf{r}) = A_0 \frac{W_0}{W(z)} \exp\left(-\frac{\rho^2}{W^2(z)}\right) \exp\left(-jkz - jk \frac{\rho^2}{2R(z)} + j\zeta(z)\right) \quad (4.19)$$

where

$W_0$  is the minimum waist value at  $z = 0$  and it is defined as

$$W_0 = \left( \frac{\lambda z_0}{\pi} \right)^{\frac{1}{2}} \quad (4.20)$$

$W(z)$  is the waist value at  $z$  and can be written as following

$$W(z) = W_0 \left[ 1 + \left( \frac{z}{z_0} \right)^2 \right]^{\frac{1}{2}} \quad (4.21)$$

$R(z)$  is the radius of curvature and its expression is given by

$$R(z) = z \left[ 1 + \left( \frac{z_0}{z} \right)^2 \right] \quad (4.22)$$

$\zeta(z)$  is the excess phase

$$\zeta(z) = \arctan \frac{z}{z_0} \quad (4.23)$$

$z_0$  is the Rayleigh range, and the radial distance is defined as  $\rho^2 = x^2 + y^2$ .

#### 4.4.2 Grating Formation by Interference of Two Gaussian Beams Travelling in Arbitrary Direction

Let us suppose that two Gaussian beams travelling in arbitrary directions are being interfered at  $z = 0$  plane as shown in figure 4.4

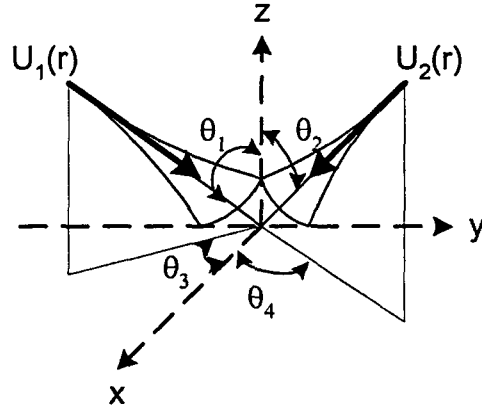


**Figure 4.4** Interference Geometry of Gaussian Beams

According to the geometry, shown in figure 4.4, the Gaussian beams can be defined as following

$$U_1(x, y, z; \theta_1, \theta_2) = A_1 \exp\left(-\frac{x_1^2 + y_1^2}{W_1^2(z)}\right) \exp\left(jk_1 \frac{x_1^2 + y_1^2}{2R_1(z)}\right) \times \exp(jk_1(z_1 - zb_1) - jk_1\zeta_1(z)) \quad (4.24)$$

$$U_2(x, y, z; \theta_3, \theta_4) = A_2 \exp\left(-\frac{x_2^2 + y_2^2}{W_2^2(z)}\right) \exp\left(jk_2 \frac{x_2^2 + y_2^2}{2R_2(z)}\right) \times \exp(jk_2(z_2 - zb_2) - jk_2\zeta_2(z)) \quad (4.25)$$

where

1-)  $\theta_1$  and  $\theta_2$  are incident angles of the beams  $U_1(r)$  and  $U_2(r)$  with respect to  $z$  axis

2-)  $\theta_3$  and  $\theta_4$  are angles between  $x$  axis and projections of incident beams  $U_1(r)$  and  $U_2(r)$ , respectively.

3-)  $A_1$  and  $A_2$  are constants, which can be defined as

$$A_{1,2} = \frac{A_{11,22}}{jz_{01,02}}$$

where  $A_{11}$  and  $A_{22}$  are constants, too.

4-)  $[x_1, y_1, z_1]$  and  $[x_2, y_2, z_2]$  are the new coordinate systems, obtained after the rotation of  $[x, y, z]$  coordinate system in order to coincide the propagation direction of beams  $U_1(r)$  and  $U_2(r)$  with  $z$  axis, respectively. According to this transformation, the new coordinate systems can be written as

$$x_1 = x \cos \theta_1 \cos \theta_3 + y \cos \theta_1 \sin \theta_3 - z \sin \theta_1 \quad (4.26a)$$

$$y_1 = -x \sin \theta_3 + y \cos \theta_3 \quad (4.26b)$$

$$z_1 = x \sin \theta_1 \cos \theta_3 + y \sin \theta_1 \sin \theta_3 + z \cos \theta_1 \quad (4.26c)$$

and

$$x_2 = x \cos \theta_2 \cos \theta_4 + y \cos \theta_2 \sin \theta_4 - z \sin \theta_2 \quad (4.27a)$$

$$y_2 = -x \sin \theta_4 + y \cos \theta_4 \quad (4.27b)$$

$$z_2 = x \sin \theta_2 \cos \theta_4 + y \sin \theta_2 \sin \theta_4 + z \cos \theta_2 \quad (4.27c)$$

The Gaussian beam parameters must be also modified. This leads to

$$W_{1,2}(z) = W_{01,02} \left[ 1 + \left( \frac{z_{1,2} - zb_{1,2}}{z_{01,02}} \right)^2 \right]^{\frac{1}{2}} \quad (4.28)$$

$$R_{1,2}(z) = |z_{1,2} - zb_{1,2}| \left[ 1 + \left( \frac{z_{01,02}}{z_{1,2} - zb_{1,2}} \right)^2 \right] \quad (4.29)$$

$$W_{01,02} = \left( \frac{\lambda_{1,2} \times z_{01,02}}{\pi} \right)^{\frac{1}{2}} \quad (4.30)$$

$$\zeta_{1,2}(z) = \arctan \frac{z_{1,2} - zb_{1,2}}{z_{01,02}} \quad (4.31)$$

where  $zb_{1,2}$  are initial points of Gaussian beams in transformed coordinate system and  $z_{01}, z_{02}$  are the Rayleigh range of each beam.

Let assume that Gaussian beams, shown in figure 4.4 have frequencies  $w_1$  and  $w_2$ . Thus, they can be written in the following form



$$U_1(r, t) = U_1(r)e^{(-j\omega t)} + \text{c.c} \quad (4.32a)$$

$$U_2(r, t) = U_2(r)e^{(-j\omega_2 t)} + \text{c.c.} \quad (4.32b)$$

It is obvious that Gaussian beam is an even function, thus any Gaussian wave can be defined in the form

$$U(r, t) = \frac{1}{2}(U(r, t) + U^*(r, t)) \quad (4.33)$$

By using the eq.(4.33) the interference equation can be written as

$$\begin{aligned} I(x, y, z, t) &= |U_1(r, t) + U_2(r, t)|^2 = \\ &= U_1(r, t)U_1^*(r, t) + U_2(r, t)U_2^*(r, t) + U_1(r, t)U_2^*(r, t) + U_1^*(r, t)U_2(r, t) \end{aligned} \quad (4.34)$$

By substituting eq.(4.32) into eq.(4.34), we obtain the total interference equation

$$\begin{aligned} I(x, y, z, t) &= \frac{1}{2} \left( \frac{A_{11}}{z_{01}} \right)^2 \exp \left( -2 \frac{x_1^2 + y_1^2}{W_1^2(z)} \right) \left[ 1 - \frac{1}{2} \cos \left( 2k_1 \left( \frac{x_1^2 + y_1^2}{2R_1(z)} + z_1 - zb_1 + \varsigma_1 \right) - 2\omega_1 t \right) \right] + \\ &+ \frac{1}{2} \left( \frac{A_{22}}{z_{02}} \right)^2 \exp \left( -2 \frac{x_2^2 + y_2^2}{W_2^2(z)} \right) \left[ 1 - \frac{1}{2} \cos \left( 2k_2 \left( \frac{x_2^2 + y_2^2}{2R_2(z)} + z_2 - zb_2 + \varsigma_2 \right) - 2\omega_2 t \right) \right] \\ &+ \frac{A_{11}A_{22}}{z_{01}z_{02}} \exp \left[ - \left( \frac{x_1^2 + y_1^2}{W_1^2(z)} + \frac{x_2^2 + y_2^2}{W_2^2(z)} \right) \right] \times \\ &\times \left[ \begin{aligned} &\cos \left[ k_1 \frac{x_1^2 + y_1^2}{2R_1(z)} - k_2 \frac{x_2^2 + y_2^2}{2R_2(z)} + k_1(z_1 - zb_1) - k_2(z_2 - zb_2) + (k_1\varsigma_1 - k_2\varsigma_2) + (\omega_2 - \omega_1)t \right] \\ &- \cos \left[ k_1 \frac{x_1^2 + y_1^2}{2R_1(z)} + k_2 \frac{x_2^2 + y_2^2}{2R_2(z)} + k_1(z_1 - zb_1) + k_2(z_2 - zb_2) + (k_1\varsigma_1 + k_2\varsigma_2) - (\omega_1 + \omega_2)t \right] \end{aligned} \right] \end{aligned} \quad (4.35)$$

The pattern, shown by eq.(4.35) consists of stationary part and travelling part that contains components of  $\omega_1 + \omega_2$  and  $\omega_2 - \omega_1$  frequencies. In our case, the Gaussian beams originates from the same laser source, that is  $\omega_1 = \omega_2 = \omega$ .

On the other hand, the relation between refractive index modulation and intensity was defined in Chapter 2 as

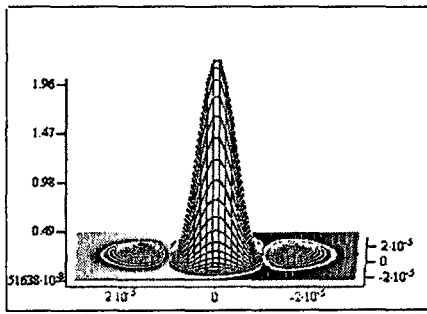
$$\Delta n = \frac{3\eta_0}{n^2 \epsilon_0} \chi^{(3)} I$$

where  $I$  represents the stationary intensity pattern

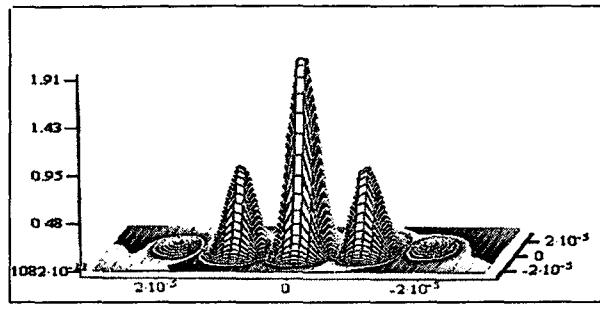
By taking into account the frequency and grating formation conditions, grating producing stationary interference pattern can be written as following

$$\begin{aligned} I_{\text{grating}} = & \frac{1}{2} \left( \frac{A_{11}}{z_{01}} \right)^2 \exp \left( -2 \frac{x_1^2 + y_1^2}{W_1^2(z)} \right) + \\ & + \frac{1}{2} \left( \frac{A_{22}}{z_{02}} \right)^2 \exp \left( -2 \frac{x_2^2 + y_2^2}{W_2^2(z)} \right) + \\ & + \frac{A_{11} A_{22}}{z_{01} z_{02}} \exp \left[ - \left( \frac{x_1^2 + y_1^2}{W_1^2(z)} + \frac{x_2^2 + y_2^2}{W_2^2(z)} \right) \right] \times \\ & \times \cos \left[ k_1 \frac{x_1^2 + y_1^2}{2R_1(z)} - k_2 \frac{x_2^2 + y_2^2}{2R_2(z)} + k_1(z_1 - zb_1) - k_2(z_2 - zb_2) + (k_1 \zeta_1 - k_2 \zeta_2) \right] \end{aligned} \quad (4.36)$$

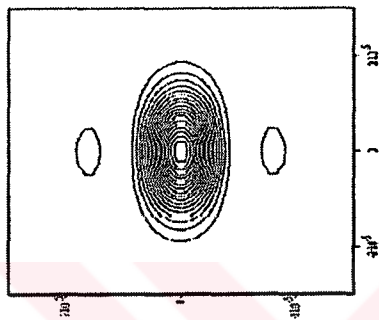
The structure of the grating for different Gaussian beam parameters is shown in Figure 4.5



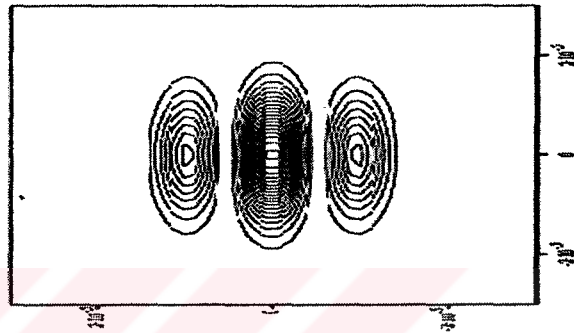
(a) Surface Plot



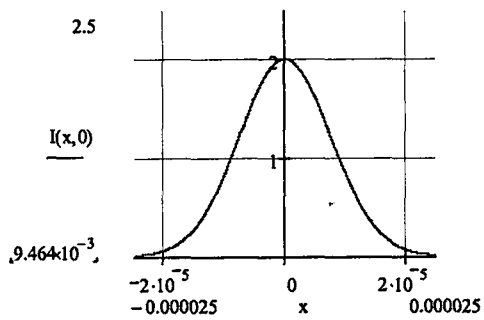
(e) Surface Plot



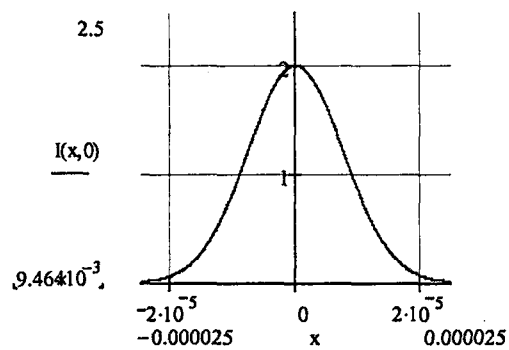
(b) Contour Plot



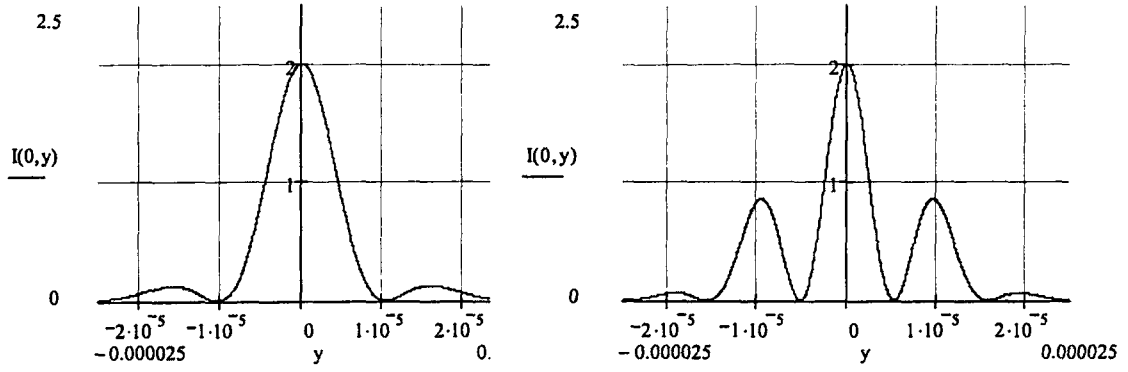
(f) Contour Plot



(c) Intensity pattern versus x when y,z = 0



(g) Intensity pattern versus x when y,z = 0



(d) Intensity pattern versus y when  $x, z = 0$  (h) Intensity pattern versus y when  $x, z = 0$   
 $= 0$

**Figure 4.5** Interference Pattern Formation And Comparison of Gratings For Different Gaussian Beam Parameters

(a) , (b) , (c) , (d) :  $zb_1 = zb_2 = 10^{-4}$  ,  $z_{01} = z_{02} = 10^{-3}$  ,  $\theta_1 = \theta_2 = \frac{\pi}{180}$  ,  $\theta_3 = \theta_4 = \frac{\pi}{2}$  e) ,

(f) , (g) , (h) :  $zb_1 = zb_2 = 10^{-4}$  ,  $z_{01} = z_{02} = 10^{-3}$  ,  $\theta_1 = \theta_2 = \frac{\pi}{90}$  ,  $\theta_3 = \theta_4 = \frac{\pi}{2}$

### 4.4.3 First Order Approximation

In the previous section, grating forming interference pattern were obtained for Gaussian beams travelling in arbitrary directions. But this definition is too complex to be used in analytical expressions and should be simplified.

The form of the complex amplitude of Gaussian beam travelling in the z direction was defined in eq. (4.1). It can be simplified and written as

$$E(z) = A \frac{\exp(-jkz)}{q(z)} \exp\left[-jk \frac{\rho^2}{2q(z)}\right] \quad (4.37)$$

where

$$\frac{1}{q(z)} = \frac{1}{R(z)} - j \frac{\lambda}{\pi W^2(z)}$$

and

$$\rho^2 = x^2 + y^2$$

$W(z)$  and  $R(z)$  are beam width and wavefront radius of curvature, respectively. We may use eq.(4.37) to represent a Gaussian beam propagating at an angle  $\theta$  with respect to the  $x$ -axis in  $xz$  plane, i.e beam propagating in the  $x'$  direction.

$$E(x') = A_1 \exp[jk(x' - L)] \exp\left[jk \frac{\rho'^2}{2q(x)}\right] \quad (4.38)$$

where  $L$  is the axial distance measured between minimum waist point and origin of the interference plane, radial distance  $\rho'^2 = (z')^2 + y^2$  and  $q(x') = (x' - L) - jx'_0$ . After coordinate transformation complex amplitude of the Gaussian beam takes the following form

$$U(r) = \frac{A}{q(x, \theta)} \exp[jk((z - L \sin \theta) \sin \theta + (x - L \cos \theta) \cos \theta)] \exp\left[j \frac{|k| \rho'^2}{2q(x, \theta)}\right] \quad (4.39)$$

where

$$q(x, \theta) = x \sqrt{1 + \tan^2 \theta} - L - jx'_0.$$

Since  $\theta$  is very small due to 3D structure of the node, it is appropriate to use first order approximation that yields the result below:

$$\sin \theta \cong \theta - \frac{1}{3!} \theta^3 \approx \theta \quad (4.40)$$

$$\cos \theta \cong 1 - \frac{1}{2!} \theta^2 \approx 1 \quad (4.41)$$

$$\tan^2 \theta \cong \theta^2 \approx 0 \quad (4.42)$$

By substituting these equations into eq.(4.39), we obtain

$$U(r) = \frac{A}{q(x, \theta)} \exp[jk((z - L\theta) \theta + (x - L))] \exp\left[j \frac{|k| \rho'^2}{2q(x, \theta)}\right] \quad (4.43)$$

where

$$q(x, \theta) = x - L - jx'_0 \quad (4.44a)$$

$$\rho'^2 = (z - x\theta)^2 \quad (4.44b)$$

Then, the general Gaussian beam expression travelling at an small angle with respect to the x axis can be defined as follows

$$U(x, z, \theta) = \frac{A}{q(x)} \exp \left[ jk \left( \eta(x, z, \theta) + \frac{\Phi}{2q(x)} \right) \right] \quad (4.45)$$

where

$$\eta(x, z, \theta) = \begin{cases} \eta_+(x, z, \theta) \cong z\theta + x - L, \theta > 0 \\ \eta_-(x, z, \theta) \cong -z\theta + x - L, \theta < 0 \end{cases} \quad (4.46)$$

$$\Phi = \begin{cases} \Phi_+ \cong z(z - 2x\theta), \theta > 0 \\ \Phi_- \cong z(z + 2x\theta), \theta < 0 \end{cases} \quad (4.47)$$

$$q(x) = \begin{cases} q = x - L - jx'_0, \theta > 0 \\ q^* = x - L + jx'_0, \theta < 0 \end{cases} \quad (4.48)$$

As shown in figure 4.5, the grating is created by the interference of the waves with wavenumbers  $k_1$  and  $k_2$ . The interference equation consists of  $|E_1|^2$ ,  $|E_2|^2$ ,  $E_1 \cdot E_2^*$

and  $E_1^* \cdot E_2$  terms as defined in eq.(4.34), where the first two terms  $|E_1|^2$  and  $|E_2|^2$  are DC components, and last two terms have the same pattern. Thus, we may assume that  $E_1.E_2^*$  represents the grating pattern in the FWM equations. By using equations (4.33) and (4.45) the electric field of grating forming beams can be written in the following form

$$E_1 = \frac{A_1}{2q} \exp\left[j|k|\left(\eta_+ + \frac{\Phi_+}{2q}\right) + \omega_0 t\right] + \frac{A_1^*}{2q^*} \exp\left[-j|k|\left[\eta_+ + \frac{\Phi_+}{2q^*}\right] + \omega_0 t\right] \quad (4.49)$$

$$E_2^* = \frac{A_2}{2q^*} \exp\left[-j|k|\left(\eta_- + \frac{\Phi_-}{2q^*}\right) + \omega_0 t\right] + \frac{A_2}{2q} \exp\left[j|k|\left(\eta_- + \frac{\Phi_-}{2q}\right) + \omega_0 t\right] \quad (4.50)$$

Assuming that  $A_1=A_2=A$  and phase delay as  $\delta$ , it is evident that

$$E_1.E_2^* = \frac{2A^2}{|q|^2} \exp\left[-\frac{x_0 z^2}{|q|^2}\right] \cos\left[|k|\left[2z\theta - \frac{2zx\theta(x-1)}{|q|^2}\right] + \delta\right] + \quad (4.51)$$

$$+ \bar{A}^2 \exp\left[-\frac{x_0 z^2}{|q|^2}\right] \cos\left[|k|\left[(x-L) + \frac{z^2}{|q|}(x-L)\right] + 2\omega_0 t + \bar{\delta}\right]$$

The first term of this equation is a standing wave in the z direction and modified at the various x planes. At  $x = 0$  plane first term produces a plane wave grating  $|k|.2z$  as expected. The grating will be built up due to intensity of this term in the z-direction which cause the Floquet-Bloch wave propagation. The second term of this equation is a travelling wave in the  $-x$  direction, modified with  $z^2/|2q|$  term and it does not contribute to the grating forming process, so it will not be considered here.

Let us eliminate the travelling wave part of eq.(4.51), that leads to

$$E_1.E_2^* = \frac{2A^2}{|q|^2} \exp\left[-\frac{x_0 z^2}{|q|^2}\right] \cos\left[|k|\left[2z\theta - \frac{2zx\theta(x-1)}{|q|^2}\right] + \delta\right] \quad (4.52)$$

In figure 4.6 the grating fronts are obtained for  $x_0=5\mu\text{m}$ ,  $\lambda_0=1.0\mu\text{m}$ ,  $L=14\mu\text{m}$  (distance from the minimum waist location) and drawn on the  $xz$  plane. The slopes (slanted) of the grating fronts approaching 80 degree after a few grating period which are critical to explain the operation of the switching property. If the beams were plane waves the grating fronts would be transmission grating with a zero degree slope (horizontal line). However, the slope can be manipulated by Gaussian beam parameters  $x_0$  and  $L$  as indicated in the eq.(4.51). Here,  $x_0$  is defined by the laser output, but  $L$  can be adjusted by a simple lenslet to make slanted reflection grating as shown in figure 4.6.

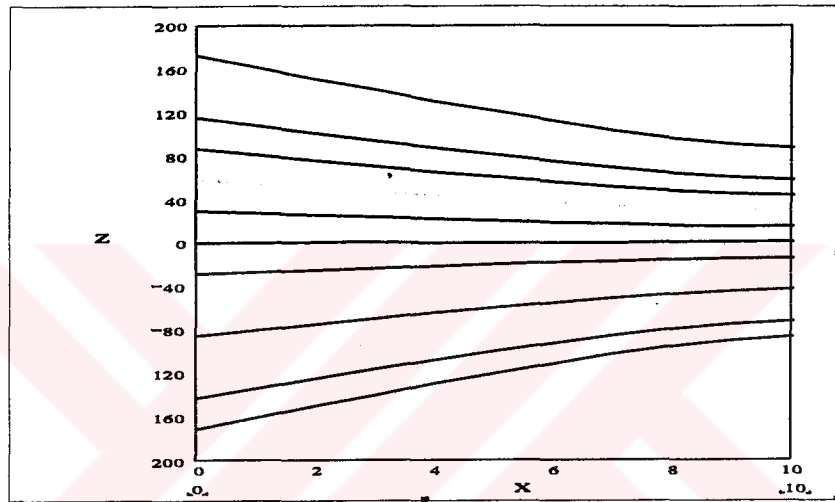


Figure 4.6 Grating Fronts

## 4.5 Coupled Wave Equations

In order the waves to be coupled, they must satisfy the matching conditions, that was defined by eq.(4.1) and eq.(4.2). Thus, this coupling waves can be written in terms of Helmholtz equation(Saleh 1991)

$$(\nabla^2 + k_4^2)E_4 = -\zeta E_1 E_3 E_2^* - \gamma_4 E_4 \quad (4.53a)$$

$$(\nabla^2 + k_3^2)E_3 = -\zeta E_2 E_4 E_1^* - \gamma_3 E_3 \quad (4.53b)$$

where



$$\zeta = 6\mu_0 w^2 \chi^{(3)} \quad (4.54a)$$

$$\gamma_3 = 3\mu_0 w^2 \chi^{(3)} (I_T - I_3) \quad (4.54b)$$

$$\gamma_4 = 3\mu_0 w^2 \chi^{(3)} (I_T - I_4) \quad (4.54c)$$

Combining eq.(4.52) and eq.(4.54) gives

$$(\nabla^2 + k_3^2)E_3 = -\zeta \text{Cos}(K(\theta, x)z) \exp(-\alpha z^2) E_4 - \gamma_3 E_3 \quad (4.55a)$$

$$(\nabla^2 + k_4^2)E_4 = -\zeta \text{Cos}(K(\theta, x)z) \exp(-\alpha z^2) E_3 - \gamma_4 E_4 \quad (4.55b)$$

where

$$K(\theta, x) = 2k \sin(\theta) \left[ 1 - \frac{x(x-L)}{(x-L)^2 + X_0^2} \right] \quad (4.56)$$

$$\alpha = -\frac{X_0^2}{(x-L)^2 + X_0^2} \quad (4.57)$$

The total field in the perturbed waveguide can be written as the superposition of the modes as defined in eq.(3.10)

$$E_3 = \sum_1 A_1(z) E_1(x, y) \exp(-j\beta_1 z) \quad (4.58a)$$

$$E_4 = \sum_k B_k(z) E_k(x, y) \exp(-j\beta_k z) \quad (4.59b)$$

Introducing eq.(4.58) into eq.(4.55) and using slowly varying approximations, we obtain the coupled mode equations

$$\frac{\partial A_1}{\partial z} = -j\zeta \frac{\beta_1}{|\beta_1|} C_{1k} B_k e^{-\alpha z^2} e^{-j\Delta\beta z} e^{j\delta_1 z} \quad (4.60a)$$

$$\frac{\partial B_k}{\partial z} = -j\zeta \frac{\beta_k}{|\beta_k|} C_{k1} A_1 e^{-\alpha z^2} e^{j\Delta\beta z} e^{j\delta_k z} \quad (4.60b)$$

where

$$\delta_i = 3\mu w^2 \chi^{(3)} \frac{(I_T - I_i)}{2\beta_i} \quad (4.61)$$

$$\Delta\beta = \beta_k - \beta_i \quad (4.62)$$

$$C_{ki} = \int E_k^* \cos(K(\theta, x)z) E_i dx \quad (4.63)$$

The coupling equation parameters  $\delta$  and  $C_{ki}$  are very important in describing the efficiency of the switching node.  $\delta$  depends on total power of incident waves, that by arranging the laser power it can be used as a tuning parameter of the coupling. Whereas, coupling coefficient can be calculated by using eq.(4.63), but it is obvious that the result will strongly depend on the geometry of the grating pattern. In order to overcome this drawback, coupling coefficient can be found by using Distributed Feedback Laser model defined in chapter 3.3 .

## 4.6 Overall Efficiency Using DFB Approach

Let us find a solution to the coupling equations near  $z = 0$  point, shown in Figure 4.6 . At that interval, we may possess a slowly varying envelop approximation, that leads to

$$\begin{aligned} \frac{\partial A_i}{\partial z} &= -j\zeta \frac{\beta_i}{|\beta_i|} C_{ik} B_k e^{-j\Delta\bar{\beta}z} \quad 4.64a \\ \frac{\partial B_k}{\partial z} &= -j\zeta \frac{\beta_k}{|\beta_k|} C_{ki} A_i e^{j\Delta\bar{\beta}z} \quad (4.64b) \end{aligned}$$

By using power conservation condition  $\frac{d}{dz} (|A_i|^2 + |B_k|^2) = 0$  and  $A_i(z) = 0$ , we can find the fraction of power that is coupled from A to B in a distance z, that is output of the transient grating

$$\frac{|B_k(z)|^2}{|A_i(0)|^2} = \frac{|C_{ki}|^2}{|C_{ki}|^2 + \Delta\bar{\beta}^2} \sin^2 \left( \sqrt{|C_{ki}|^2 + \Delta\bar{\beta}^2} z \right) \quad (4.65)$$

where

$$\Delta\bar{\beta} = \beta_k - \beta_1 + \delta \pm mK = 0 \quad (4.66)$$

The coupling equation parameters  $\delta$  and  $C_{kl}$  are very important in describing the efficiency of the switching node.  $\delta$  depends on total power of incident waves, that by arranging the laser power it can be used as a tuning parameter of the coupling. Whereas, coupling coefficient can be calculated by using eq.(4.63), but it is obvious that the result will strongly depend on the geometry of the grating pattern. In order to overcome this drawback, coupling coefficient can be found by using Distributed Feedback Laser model defined in chapter 3.3 .

Let us consider that the matching condition is satisfied, i.e  $\Delta\bar{\beta} = 0$  . Thus, the power ratio can be written as

$$\frac{|B_k(z)|^2}{|A_1(0)|^2} = \sin^2(C_{kl}|z|) \quad (4.67)$$

In order to find the overall efficiency of the system, let us divide the nonperiodic grating shown in figure 4.6 into parts so that the length of each segment is  $\Delta z$  as shown in figure 4.7 .

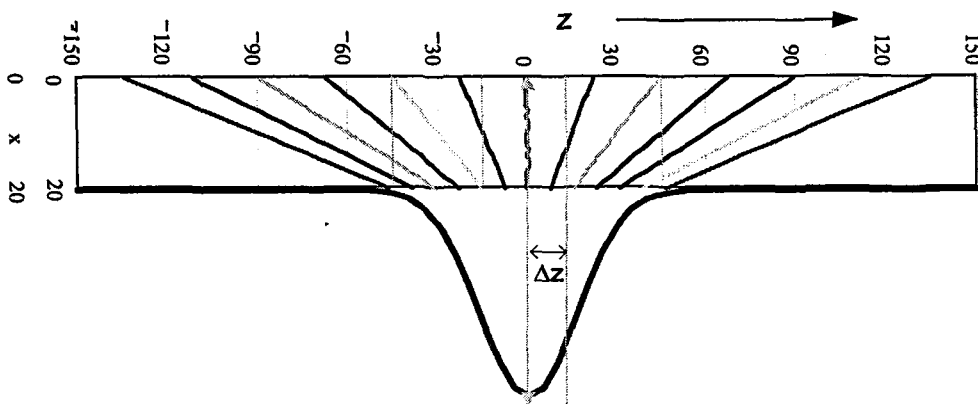


**Figure 4.7** Gaussian Grating Structure

Then, then the total power transfer ratio can be written by using the transfer ratio of each layer

$$\frac{|B_k(z)|^2}{|A_1(0)|^2} = \prod_i \sin^2 |C_{kl}|_i \Delta z_i \quad (4.68)$$

where  $|C_{kl}|_i$  is the coupling coefficient of each segment. By using the identity

$$\sin^2 A = \frac{1}{2}(1 - \cos(2A))$$

eq. (4.68) can be written in the following form

$$\begin{aligned} \frac{|B_k(z)|^2}{|A_1(0)|^2} &= \prod_i \frac{1}{2} (1 - \cos(2|C_{kl}|_i \Delta z_i)) = \\ &= \left( \frac{1}{2} (1 - \cos(2C_1 \Delta z_1)) \times \frac{1}{2} (1 - \cos(2C_2 \Delta z_2)) \times \frac{1}{2} (1 - \cos(2C_3 \Delta z_3)) \dots \right) \end{aligned} \quad (4.69)$$

We defined coupling coefficient in eq. (4.31) as  $C = \sqrt{\eta} B_m$ , thus placing it in eq.(4.69) leads to

$$\frac{|B_k(z)|^2}{|A_1(0)|^2} = \left( \frac{1}{2} (1 - \cos(2\sqrt{\eta_1} B_1 \Delta z_1)) \times \frac{1}{2} (1 - \cos(2\sqrt{\eta_2} B_2 \Delta z_2)) \times \frac{1}{2} (1 - \cos(2\sqrt{\eta_3} B_3 \Delta z_3)) \dots \right) \quad (4.70)$$

where  $\eta_i$  is the diffraction efficiency of each grating segment and  $B_i$  is the bounce rate defined by eq. (3.32).

We computed the reflection efficiency of the grating for  $n_1=1.4801$ ,  $n_2=1.465$  and  $\Delta n=0.01$ , shown in figure 4.8 by using standard grating solving software package GSOLVER.  $R_0$  and  $R_{-1}$  correspond to zero order and first order reflection coefficients, respectively. If grating exist, the guided mode of the waveguide having incident angle 81 degree at the core-cladding boundary will be deflected by the grating into  $R_{-1}$  reflection order, otherwise the mode will be total internal reflected with coefficient  $R_0$  as normal.

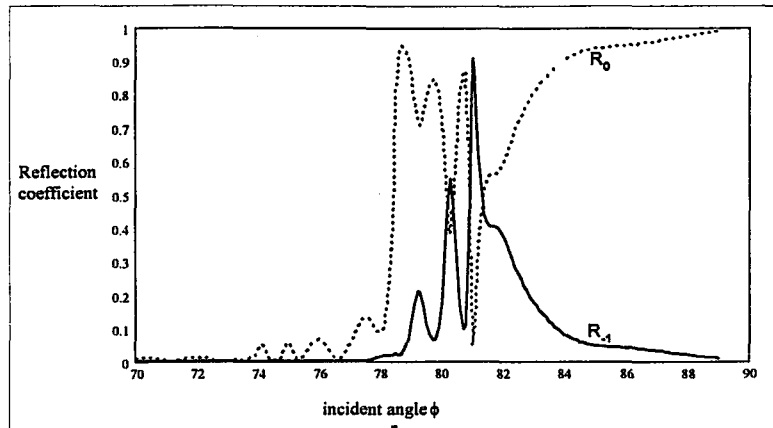


**Figure 4.8** Dependence of diffraction efficiency on the incidence angle  $\phi$ .

For the reflection efficiencies of  $\eta_1=90\%$ ,  $\eta_2=88\%$  and bounce rates of  $B_1=99\text{ cm}^{-1}$  and  $B_2=105\text{ cm}^{-1}$ , we calculated the overall efficiency as 2% by using equation 4.75. This value was obtained by assuming  $\Delta z_{1,2} = 40\mu\text{m}$  and effective thickness of the waveguide is  $w = 8\mu\text{m}$ .

## CHAPTER 5

### MEASUREMENTS AND EXPERIMENTAL STUDIES

#### 5.1 Autocorrelation Principles

The invention of ultrashort pulse lasers has introduced a new problem of direct measurement of pico and femtosecond pulses due to relatively slow response time of the detectors with respect to the pulse duration. To overcome this difficulty, an autocorrelator method was proposed and this technique have been widely used in ultrashort pulse detection applications. Figure 5.1 show a basic autocorrelator circuit

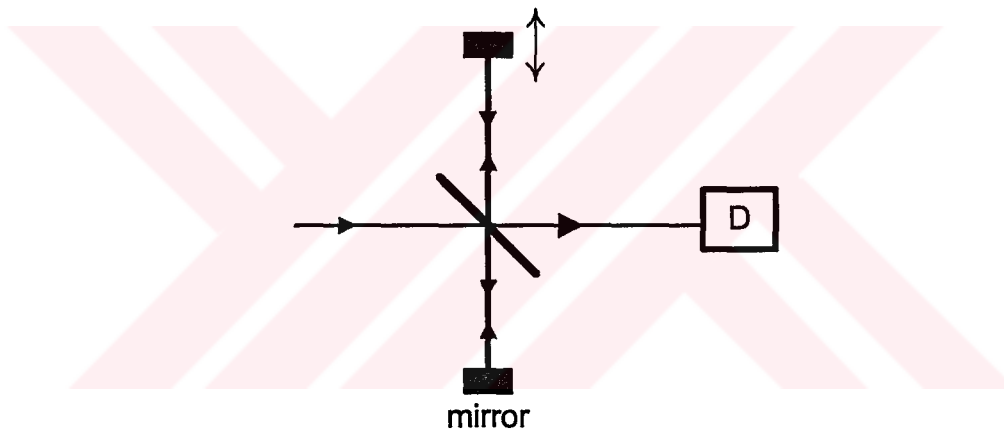


**Figure 5.1** Basic Michelson Interferometer

In this technique the laser output pulse is divided into two halves and after being reflected from the mirrors, they are correlated with each other. The temporal delay of one of the pulses is obtained by changing the distance (by moving mirror on translation stage) it travels in the arm of the interferometer.

There are two types of autocorrelation, intensity and interferometric autocorrelation, called slow and fast respectively. Let us consider the Michelson interferometer, shown in figure 5.1 and assume that the real electric field at the input of the detector is

$$E = E_1(t - \tau) + E_2(t) \quad (5.1)$$

where  $\tau$  is the temporal delay obtained by moving the mirror. The signal at the input of

the detector is a second order interferometric correlation, which is defined as (Diels 1996]

$$G_2(\tau) = \int_{-\infty}^{\infty} \{[E_1(t-\tau) + E_2(\tau)]^2\}^2 dt \quad (5.2)$$

The electric field E can be described as

$$E = E(t)e^{i(\omega t - \phi(t))} \quad (5.3)$$

Putting this field into eq. (5.2) leads to

$$G_2(\tau) = A(\tau) + \text{Re}\{4B(\tau)e^{i\omega\tau}\} + \text{Re}\{2C(\tau)e^{i2\omega\tau}\} \quad (5.4)$$

where

$$A(\tau) = \int_{-\infty}^{\infty} \{E_1^4(t-\tau) + E_2^4(t) + 4E_1^2(t-\tau)E_2^2(t)\} dt \quad (5.5)$$

$$B(\tau) = \int_{-\infty}^{\infty} \{E_1(t-\tau)E_2(t)[E_1^2(t-\tau) + E_2^2(t)]e^{i(\phi_1(t-\tau) - \phi_2(t))}\} dt \quad (5.6)$$

$$C(\tau) = \int_{-\infty}^{\infty} \{E_1^2(t-\tau)E_2^2(t)\}e^{i2(\phi_1(t-\tau) - \phi_2(t))} dt \quad (5.7)$$

If the response of the autocorrelator is slow compared to the duration of one optical cycle, then the information in the interferometric correlation will be time average of  $G_2(\tau)$ , that is  $A(\tau)$ . This is the intensity autocorrelation. Unlike the interferometric, no phase information is contained within intensity autocorrelations.

Previously, nonlinear crystal and photomultiplier was the most common combination to detect autocorrelated signal. Recently, it was discovered that photodiodes which exhibit nonlinear power dependent response can be used to detect and to characterise ultrashort pulses. The mechanism for the nonlinear effect in photodiodes is two photon absorption (TPA).

## 5.2 Two Photon Absorption In Semiconductor Photodiodes

Two photon absorption ( TPA ) is a nonresonant nonlinear process that occurs for photons with energy  $h\nu$  less than the semiconductor energy gap  $E_g$ , but greater than  $E_g / 2$ . For this range of photon energies, there is very little absorption of light due to absorption of single photon. However, when a semiconductor is illuminated by an intense beam, an electron can be excited from the valence band to the conduction band by the absorption of two photons. Due to need of high intensity light, TPA was not observed until the invention of the laser, but its existence has been predicted earlier(Laughton 1994)

For photon energies less than  $E_g$ , but greater than  $E_g / 2$ , the main carriers will be generated by TPA process and this can be measured as a photocurrent. Because of the two photon nature of the interaction, the photocurrent will be a quadratic function of the light intensity(Laughton 1994)

In order to be able to use a nonlinear optical effect for pulsewidth measurements, the response time of the nonlinearity must be much less than the pulswidth to be measured. Consider the configuration in Figure 5.2 and assume that the laser output is continuous wave beam.

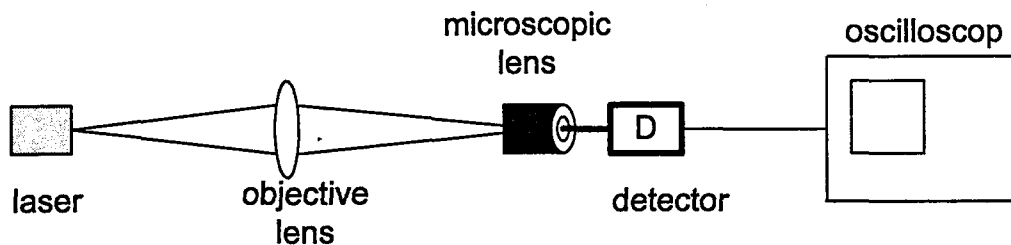


Figure 5.2 Two photon absorption experiment setup

For a single CW beam, the carrier photogeneration rate is[LAUGHTON]

$$\left[ \frac{dN}{dt} \right]_{ave} = \frac{\alpha}{h\nu} I_{ave} + \frac{\beta}{h\nu} I_{ave}^2 \quad (5.8)$$



where  $I_{ave}$  is the average intensity of the beam,  $h\nu$  is the photon energy,  $\beta$  is the two photon absorption coefficient and  $\alpha$  is the one photon absorption coefficient.

The average photocurrent can be written as

$$(J_{ph})_{CW} = e\Omega \left( \frac{\alpha}{h\nu} I_{ave} + \frac{\beta}{h\nu} I_{ave}^2 \right) \quad (5.9)$$

where  $e$  is the electronic charge and  $\Omega$  is the volume in which the carriers are created.

If we consider the pulse laser, we can assume that Gaussian intensity profile is given by

$$I(t) = I_p e^{-\frac{2t^2}{T^2}} \quad (5.10)$$

where  $I_p$  is the peak intensity of the pulse and its relation with the average intensity is defined as

$$I_p = I_{ave} \sqrt{\frac{2}{\pi}} \frac{t_p}{T} \quad (5.11)$$

Then, the average photocurrent for the pulsed beam is

$$(J_{ph})_{pulse} = \frac{e\Omega}{t_p} \int_{-\infty}^{\infty} \frac{dN}{dt} dt \quad (5.12)$$

$$J_{ph} = e\Omega \left( \frac{\alpha}{h\nu} I_{ave} + \frac{\beta t_p}{2\sqrt{\pi} h\nu T} I_{ave}^2 \right) \quad (5.13)$$

where  $t_p$  is the time between laser pulses.

In order to calculate the output current of the detector in autocorrelator as shown in figure 5.3, let us consider a two pulses having Gaussian profile and travelling in the arms of the interferometer with time delay  $\tau$  with respect to each other.

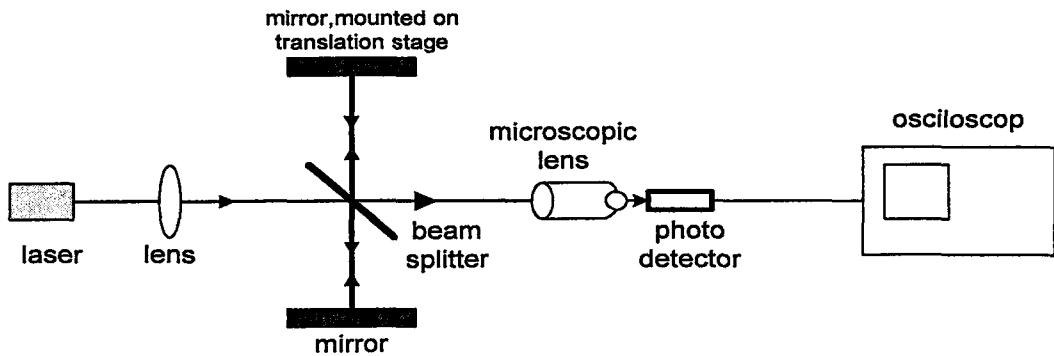


**Figure 5.3** Autocorrelator experiment setup

Let us assume that beams are orthogonally polarized that will prevent interference effect. By using these assumptions, the instantaneous intensity just in front of photodiode can be written as

$$I(t) = I_p e^{-\frac{2t^2}{\tau^2}} + I_p e^{-\frac{2(t-\tau)^2}{\tau^2}} \quad (5.14)$$

The average carrier generation rate is written as

$$\left(\frac{dN}{dt}\right)_{\text{ave}} = \frac{1}{\tau_p} \int_{-\infty}^{\infty} \left( \frac{\alpha}{h\nu} I(t) + \frac{\beta}{2h\nu} I^2(t) \right) \quad (5.15)$$

and the average photodiode current as a function of the time delay  $\tau$  between pulses is given by

$$I_{\text{ph}}(\tau) = e\Omega \left( \frac{2\alpha}{h\nu} I_{\text{ave}} + \frac{\beta t_p}{\sqrt{\pi h\nu T}} I_{\text{ave}}^2 \right) \left( 1 + e^{-\frac{t_d^2}{\tau^2}} \right) \quad (5.16)$$

In order to obtain the true pulsewidth, the photocurrent value must be divided by  $\sqrt{2}$  due to Gaussian nature of the pulse.

## CHAPTER 6

### CONCLUSION

The analysis carried out here are based on FWM and ray approach to identify the reflection angle and efficiency of the node system. For a transient grating formed by the plane waves, a mode incident at an angle  $81.9^\circ$  is reflected from grating at an angle  $69.9^\circ$ , that is obtained for a sinusoidal spatial period of  $19.55\mu\text{m}$ . Furthermore, to find the efficiency of the proposed model, the transient grating is assumed to be formed in the core-cladding and considered that it is purely slanted reflection grating, that is a rough approximation to real shape. Although the grating period and slant angle change with  $x$  and in the  $z$ -direction, it converges quickly a stable angle value of about  $80^\circ$  degree in our case. The grating strength degrades with  $\exp(-az^2)$  in the  $z$ -direction as given in eq.(4.52). Therefore, the effective grating is in fact formed in a limited area, which may dramatically affects the total reflected power.

By performing a coupled wave analysis of proposed model, a nearly 2% overall efficiency is calculated for the switching node. This efficiency may be increased considerably by applying some optimization on the designed node. First of all, the coupling coefficient described in eq.(4.63) depends strongly on the geometry chosen for the unperturbed waveguide and transient grating structure. In the standard coupled wave analysis, the grating is defined in term of Fourier series and the solution is obtained by neglecting higher order terms. To obtain a more compact solution to coupling efficiency, we used a geometry independent method to find the coupling coefficient. In this method, the nonperiodic grating was divided into layers with width  $\Delta z$  so that strength of the grating remains unchanged within the selected segment. In this layer, instead of solving the overlap integral, DFB approach is used to obtain the coupling coefficient of the related segment. Thus, the overall efficiency is the multiplication of the efficiency of the each layer.

The results obtained in this thesis show a great correspondence between the Gaussian beam parameters  $L$ ,  $x_0$ , incidence angle  $\theta$ , the intensities of grating forming beams and overall efficiency. All of these vaues are tuning parameters, that can be used to improve the diffraction efficiency. For example, the choice of the layer width  $\Delta z$

depends on grating strength, which is completely determined by Gaussian beam parameters. Regarding to eq.(4.70), more efficient results is obtained by increasing the interaction length  $\Delta z$ . Furthermore, the efficiency equation described in eq. (4.70) is obtained for a constant spatial frequency through x axis. In fact, the nonperiodic grating consists of a number of components and one can write the coupling equations for each component and obtain more efficient result. Nevertheless, other parameters that have influence on the efficiency of the system like reflection of the grating forming beams, scattering and absorption of the nonlinear material surface are not considered at all.

Finally, a detailed experimental study should be carried on to verify the theoretical results obtained in this thesis and this verification will ensure the applicability of the method to develop an all optical switch.



## REFERENCES

### Book:

- Boyd, R.W., 1992. "Nonlinear Optics", (Academic Press, San Diego).
- Diels, J.C., 1996. "Ultrashort Laser Pulse Phenomena", (Academic Press, San Diego).
- Sakoda, K., 2001. "Optical Properties of Photonic Crystals", (Springer, Germany).
- Saleh, B.E.A., 1991. "Fundamentals of Photonics", (JohnWiley & Sons , USA).
- Yariv, A, Yeh, P., 1984. "Optical Waves in Crystals", (JohnWiley & Sons, New York).
- Yariv, A., 1997. "Optical Electronics in Modern Communications", (Oxford University Press, New York).

### Periodical Article:

- Babbit, R.A., Mossberg, T.W., 1998. "Optical Waveform Processing and Routing with Structured Surface Gratings", *Optics Communications*, 148, 23-26
- Fishman, I. M., Marshall, C. D., Meth, J. S., Fayer, M. D., 1991. "Surface Selectivity in Four Wave Mixing: Transient Gratings as Theoretical and Experimental Example", *J. Opt. Soc. Am. B*, Vol.8, No.9.
- Hamad, A.Y., Wicksted, J.P. , 1997, "Volume Grating Produced by Intersecting Gaussian Beams in an Absorbing Medium: a Bragg Diffraction Model", *Optics Communications*, 138, 354-364.
- Laughton, F.R, Marsh, J.H., Barrow, D.A., 1994. "The Two Photon Absorption Semiconductor Waveguide Autocorrelator", *IEEE Journal of Quantum Electronic*, Vol.30, No:3.
- Luo, H.J., Zory, P.S., 1994. "Ray Optics Determination of the DFB Coupling Coefficient in Separate Confinement and Multi-quantum Well Laser Structures", *IEEE Journal of Quantum Electronic*, Vol.30, No:1.

Self Phase Matching Through a Transient Kerr Grating and the Way to Ultrafast Computing”, Appl. Phys. B 74, 745-748.

Schneider, T., Schmid, R.P, Mitzner, R., Reif, J. 2000. “Femtosecond Index Grating in Barium Flouride: Efficient Self Diffraction and Enhancement of Surface SHG”, Applied Surface Science 154-155, 565-570

Zheng, Z., Weiner, A.M., Marsh, J., Karkhanechi, M.M., 1997. “Ultrafast optical Thresholding Based on Two Photon Absorption GaAs Waveguide Photodetectors”, IEEE Photonics Technology Letters, Vol.9, No:4

